Cell

Prediction of Photoperiodic Regulators from Quantitative Gene Circuit Models

José Domingo Salazar,[1,2,3,7] Treenut Saithong,[5] Paul E. Brown,[3,5] Julia Foreman,[5] James C.W. Locke,[1,3,4,8] Karen J. Halliday,[5] Isabelle A. Carré,[1] David A. Rand,[2,3] and Andrew J. Millar[5,6,*]

[1]Department of Biological Sciences
[2]Mathematics Institute
[3]Interdisciplinary Programme for Cellular Regulation and Warwick Systems Biology Centre
[4]Department of Physics
University of Warwick, Coventry CV4 7AL, UK
[5]School of Biological Sciences, Edinburgh University, Mayfield Road, Edinburgh EH9 3JH, UK
[6]Centre for Systems Biology at Edinburgh, C.H.Waddington Building, King's Buildings, Edinburgh EH9 3JR, UK
[7]Present address: Human Safety, Syngenta, Jealott's Hill International Research Centre, Bracknell, Berkshire RG42 6EY, UK
[8]Present address: Division of Biology, California Institute of Technology, 1200 E. California Blvd., Pasadena, CA 91125, USA
*Correspondence: andrew.millar@ed.ac.uk
DOI 10.1016/j.cell.2009.11.029

SUMMARY

Photoperiod sensors allow physiological adaptation to the changing seasons. The prevalent hypothesis is that day length perception is mediated through coupling of an endogenous rhythm with an external light signal. Sufficient molecular data are available to test this quantitatively in plants, though not yet in mammals. In *Arabidopsis*, the clock-regulated genes *CONSTANS (CO)* and *FLAVIN, KELCH, F-BOX* (*FKF1*) and their light-sensitive proteins are thought to form an external coincidence sensor. Here, we model the integration of light and timing information by *CO*, its target gene *FLOWERING LOCUS T (FT)*, and the circadian clock. Among other predictions, our models show that FKF1 activates *FT*. We demonstrate experimentally that this effect is independent of the known activation of *CO* by FKF1, thus we locate a major, novel controller of photoperiodism. External coincidence is part of a complex photoperiod sensor: modeling makes this complexity explicit and may thus contribute to crop improvement.

INTRODUCTION

Many eukaryotes measure changes in day length (photoperiod), in order to synchronize their life strategies with seasonal rhythms. The photoperiod sensor in vertebrates is thought to be located in the *pars tuberalis* of the pituitary gland, though its molecular mechanisms are unclear (reviewed in Hazlerigg and Loudon, 2008). Day-length perception in plants occurs in leaves, giving rise to a long-range signal. In *Arabidopsis thaliana*, a signal induced by long photoperiods controls the transition to flowering at the apical meristem. Other plant species initiate overwintering adaptations, such as bud dormancy and tuber formation, in response to short photoperiods (Thomas and Vince-Prue, 1997). Photoperiod measurement depends upon an interaction between photoreceptors and the 24 hr circadian clock. In *Arabidopsis*, the clock-controlled transcription of the B-box factor *CONSTANS* (*CO*) leads to a *CO* mRNA profile that peaks late in the day. High *CO* mRNA levels coincide largely with the light interval under long-day conditions (such as 16L:8D, a cycle of 16 hr of light and 8 hr of darkness), but are restricted to the dark phase under short days (8L:16D) (Suarez-Lopez et al., 2001). The major target of *CO*, the gene *FLOWERING LOCUS T* (*FT*), is expressed after the *CO* peak, but only when *CO* expression coincides with light (Yanovsky and Kay, 2002). This led to the hypothesis that CO may activate *FT* transcription in a light-dependent manner (reviewed in Carré et al., 2006; Imaizumi and Kay, 2006). More recently, the CO protein was shown to be unstable in darkness, partly due to interaction with COP1 (Jang et al., 2008), but to accumulate under constant white or blue light (Valverde et al., 2004). Thus, stabilization of the CO protein in the light may account for the light-dependency of CO effects on *FT*. This regulation occurs in the phloem companion cells (An et al., 2004), allowing rapid transport of the FT protein product to the apical meristem (reviewed in Kobayashi and Weigel, 2007; Turck et al., 2008). There, interaction with the meristem-specific transcription factor FD activates the homeotic genes that lead to floral development (reviewed in Kobayashi and Weigel, 2007; Turck et al., 2008).

This molecular mechanism is consistent with the long-standing hypothesis that day-length perception is mediated through coincidence of an endogenous rhythm with an external light signal (Bünning, 1936). Expressing this hypothesis in equations shows that the rhythmic component could be a generic, clock-controlled gene with expression levels that rise toward the end of a long photoperiod (Oosterom et al., 2004). This contrasts with the "internal coincidence model" that may apply in vertebrates (Hazlerigg and Loudon, 2008) in which photoperiod acts to bring two circadian rhythms into a particular phase relationship (Pittendrigh, 1960). Recent evidence suggests that the mechanism of day-length perception in plants may be more complex than either conceptual model. For example, expression of the *CO* mRNA at the end of long-day photoperiods is mediated in part through the action of a rhythmically

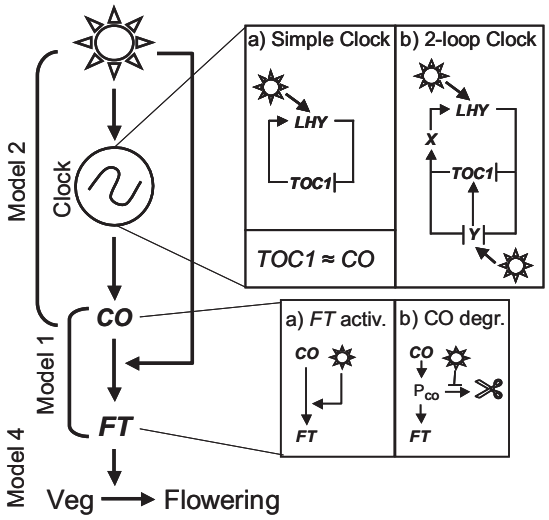

Figure 1. Overview of Modeling Stages

Model 1 uses *CO* mRNA data and light/dark cycles as inputs and simulates *FT* mRNA accumulation. In model 1a, light and *CO* mRNA activate *FT* transcription whereas in model 1b light inhibits the degradation of CO protein, which activates *FT*. Model 2 takes a light/dark cycle as input and simulates the rhythmic expression of *CO* mRNA. Model 2a is based on a single-loop model for the circadian clock (Locke et al., 2005a) while model 2b uses the interlocking-loop model (Locke et al., 2005b). Models 1 and 2 are combined in model 3, which simulates *FT* mRNA profiles for a given light/dark cycle. Speculative models including *FKF1* are presented in Figures 4, S4, S5, and S8. Model 4 uses model 3 to predict flowering responses based on *FT* mRNA accumulation.

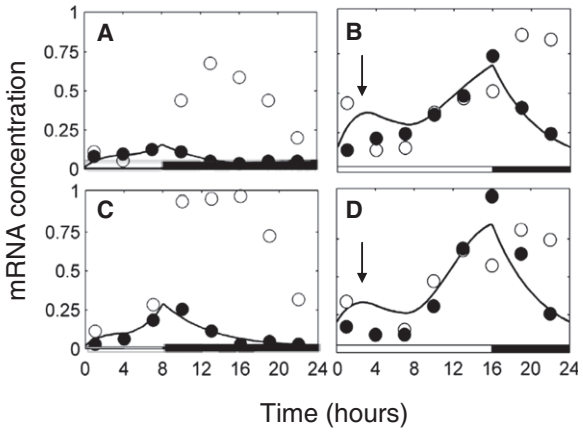

Figure 2. External Coincidence of *CO* and Light Predicts *FT* mRNA Expression

FT mRNA expression patterns were simulated using model 1a, based on the training data sets (A and B) (Yanovsky and Kay, 2002) and (C and D) (Imaizumi et al., 2003), under short-day (A and C) and long-day (B and D) conditions. The maximal *CO* mRNA level under short days is set to 1 for each set of data and simulations. Open circles, *CO* mRNA data; closed circles, *FT* mRNA data; solid line, simulated *FT* mRNA levels. Filled bar on time axis, dark interval; open bar, light interval.

expressed, light-activated F-box-Kelch protein known as FKF1 (reviewed in Imaizumi and Kay, 2006). High FKF1 protein levels coincide with the light interval at the end of a long day, when FKF1-mediated degradation of transcriptional repressors in the CYCLING DOF FACTOR family promote transcription of *CO* (Fornara et al., 2009; Imaizumi et al., 2005; Sawa et al., 2007). Under short day conditions, FKF1 is expressed in the dark and appears inactive. This external coincidence between light and the *FKF1* expression rhythm affects the *CO* expression rhythm: the level of CO protein may therefore integrate the output of two external coincidence sensors.

Here, we model the photoperiod sensor of *Arabidopsis* in detail, based upon molecular timeseries data. We aim to test whether the expression patterns of the known flowering-time genes are quantitatively consistent with their proposed regulatory functions, and whether these functions are sufficient to explain the observed behavior of the plant. Analysis of the models confirms our understanding of flowering time regulation in some areas. Specific failures of the models in other areas predict new regulatory interactions or components that can be tested by molecular experimentation.

RESULTS

Model Construction and Data Selection

The regulatory network was represented in ordinary differential equations, where the form of the equations reflected the known molecular interactions. Model construction proceeded in stages (Figure 1). Alternative models were compared at each stage. The maximal transcription rates, mRNA degradation rates and other biochemical parameters were estimated by fitting the models to quantitative, molecular timeseries data (see the Supplemental Data, available online), as none of these parameter values have been measured experimentally. The consistency of the available data sets enabled this approach. There was little data for key proteins in wild-type plants, so our initial models were based on quantitative mRNA expression patterns, with indirect information on CO protein levels and their regulation by light. Twenty-four sets of timeseries data (Table S1) were selected to construct and validate the models (see Supplemental Data).

Model 1: Activation of *FT* by *CO* and Light

Model 1 aimed to simulate the accumulation of *FT* mRNA, starting from *CO* mRNA expression data. The detailed mechanism of *FT* activation by CO protein remains to be determined, so several models were tested (Figure S1, Supplemental Data). In the simplest model (1a), we assumed that the CO protein was produced rapidly and was highly unstable, so that accumulation of the CO protein mirrored *CO* mRNA. Furthermore we supposed that the CO protein was only active in the light. Thus the rate of *FT* transcription was determined by the level of *CO* mRNA when light was present and *FT* was not transcribed in darkness. Parameter values for this model were estimated using data on *CO* and *FT* mRNA levels in wild-type plants grown under long and short photoperiods (sets 1, 3, 8, and 9, see Table S1), quantified from two publications of the Kay laboratory (Imaizumi et al., 2003; Yanovsky and Kay, 2002). We term these the training data (Figure 2). As expected, a limited number of parameter values allowed accurate simulation of the observed pattern of *FT*

mRNA accumulation (see Supplemental Data). Using the optimal parameter sets, the fit of simulated *FT* mRNA levels to either training data set was better than the fit of the experimental data sets to each other, indicating that no better match to the training data was possible.

A more complex model (1b) explicitly included an unstable CO protein that was stabilized during the light interval but rapidly degraded in darkness. Light-driven accumulation of this protein promoted *FT* transcription. Model 1b also fitted well to the training data, with no significant improvement over model 1a (unpublished data). More complex models, involving for example an additional effect of light on the ability of the CO protein to activate *FT* transcription, failed to improve the fit (see Supplemental Data). Models 1a and 1b were validated using further sets of *CO* and *FT* mRNA data from a variety of photoperiodic conditions. The parameters developed for the training data also fitted the validation data well (Figure S1C; Supplemental Data), indicating that the simple mechanisms of submodels 1a and 1b recapitulated the overall activation of *FT* by *CO*. As model 1b explicitly includes regulation of the CO protein, we anticipate that this will be more useful for comparison to future molecular data.

Modification of *FT* Activation

The quantitative models allowed us to test whether *FT* activation was altered in mutant backgrounds. The *toc1* mutation, for example, shortens the period of the circadian clock from 24 hr to 21 hr. *toc1* mutant plants are induced to flower rapidly under 8L:16D, but this defect in photoperiodism can be rescued by growing the mutants under 21 hr light-dark cycles. It was therefore proposed that the altered circadian clock function is the only photoperiod-response defect in the *toc1* mutant (Yanovsky and Kay, 2002). From the *CO* mRNA levels observed in *toc1* mutants, models 1a and 1b simulated levels of *FT* mRNA that only slightly underestimated the levels observed in *toc1* mutants (Figures S2a–S2d and unpublished data). The best match was obtained by increasing the *FT* activation parameter by 40% (Figures S2e–S2h).

Using model 1a, simulations of *FT* transcription under long days consistently predicted an aberrant peak of *FT* mRNA in the early morning that was absent from the training data (Figures 2B and 2D). The aberrant peak was also predicted using model 1b but was delayed by the time required for CO protein to accumulate (unpublished data, similar to Figure 3D). This defect suggested that our models overlooked an additional aspect of *FT* regulation. The effect of *CO* on *FT* transcription may be "gated," such that accumulation of *CO* mRNA in the morning results in less transcription of *FT* than an equal amount of *CO* mRNA in the afternoon. We estimated the effect of the hypothetical "morning gate" in model 1a and found that it was photoperiod-dependent but modest (~60% reduction in FT activation; see Supplemental Data, Figure S3). However, the RNA data available have insufficient time resolution to constrain the effect accurately, and including the morning gate made only a small contribution to the overall fit under standard long- and short-day conditions. For these pragmatic reasons and considering additional experimental evidence (see Discussion), no separate "morning gate" mechanism was included in subsequent models.

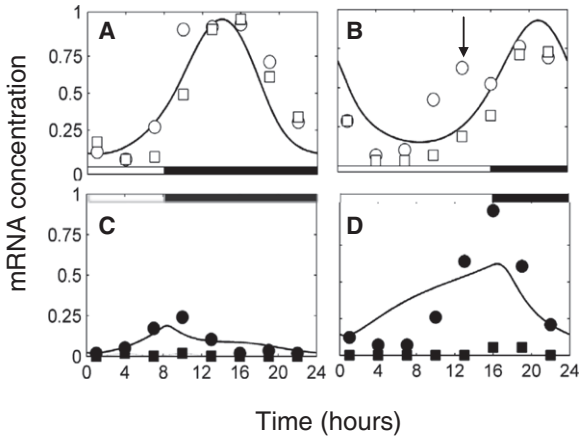

Figure 3. Model 3 Recapitulates *CO* mRNA Profiles of *fkf1* Mutant Plants but Predicts *FT* mRNA Close to Wild-Type

Expression patterns of *CO* mRNA (A and B) and *FT* mRNA (C and D) were simulated using model 3 (solid lines), under short-day (A and C) and long-day (B and D) conditions. The arrow in (B) marks the *FKF1*-dependent shoulder in *CO* expression, which is absent in the model. Expression level data (sets 8 and 9, Table S1, Imaizumi et al., 2003) are shown, as in Figure 2. Open symbols, *CO* mRNA data; filled symbols, *FT* mRNA data; circles, data from wild-type; squares, data from *fkf1* mutant. Filled bar on time axis, dark interval; open bar, light interval.

Model 2: Circadian Regulation of *CO* Transcription

The waveform of *CO* mRNA accumulation is thought to be a crucial component of the photoperiod sensor. To include rhythmic *CO* regulation in model 2, we assumed that *CO* was similar to the clock component *TOC1*, which is expressed at the same phase (Locke et al., 2006; Locke et al., 2005b). We therefore simulated *CO* expression based on the *TOC1* component of existing models for the circadian clock. Two clock models were tested. The simplest, in Model 2a, comprised a single transcriptional feedback loop and a single mechanism of light input at dawn (Figure 1) (Locke et al., 2005a). The entrained phase of this clock model is locked to dawn and the remainder of the photoperiod has no effect (Locke et al., 2006). This model fitted *CO* RNA data poorly, because it could not accommodate the observed change in the *CO* waveform between short and long photoperiods (Figure 2). In contrast, the circadian clock in Model 2b comprised two interlocking feedback loops and was entrained through light inputs to two genes (Figure 1) (Locke et al., 2005b). The interlocking-loop clock model is capable of adjusting its phase relative to dawn in response to varying photoperiods (Locke et al., 2006), resulting in a better fit to *CO* mRNA expression (Figures 3A and 3B).

Model 2b failed to predict the shoulder of *CO* mRNA accumulation that is observed at the end of the light interval under long photoperiod cycles in wild-type plants (Figure 3B, arrow). The simulated *CO* waveforms were closer to data from *fkf1* mutant plants. Since *FKF1* is known to affect *CO* mRNA accumulation at the end of a long day (Imaizumi et al., 2005, 2003; Sawa et al., 2007), the absence of *FKF1* in our model might account for this discrepancy. Under short days, where there is little difference between *CO* waveforms in wild-type and *fkf1* mutants, the model fitted both well. A preliminary model 3F1 was developed

to simulate the effect of *FKF1* on *CO* transcription, using data on the FKF1 protein profile to control additional synthesis of *CO* mRNA in a light-dependent manner (see Supplemental Data, Figure S4). The model fitted one to two time points in the shoulder of *CO* mRNA data, which had a limited effect on *FT* mRNA accumulation. Simulating an *fkf1* mutation in preliminary model 3F1 caused only a 35% reduction in *FT* transcription rate at the end of a long photoperiod. Activation of *CO* transcription by FKF1 in our model represents the double-negative mechanism, in which the CYCLING DOF FACTOR (CDF) repressor proteins are degraded by FKF1, but allows a much simpler mathematical formulation. When further quantified data become available, it should be possible to model recently-discovered details of the molecular mechanisms involved (Fornara et al., 2009; Sawa et al., 2007).

Model 3: Photoperiodic Regulation of *FT*

In order to simulate the regulation of *FT* under the control of light and the circadian clock, submodel 1b was combined with submodel 2b to form model 3 (Figure 1; see Supplemental Data). This model replaced the experimental *CO* mRNA data used in Figure 2 with the simulated *CO* mRNA waveforms shown in Figures 3A and 3B. Importantly, the model parameters were not altered, because each submodel had already been constrained to the relevant data.

The *FT* expression patterns predicted by model 3 remained consistent with the *FT* data from the training and validation data sets (Figures 3C, 3D, and S1d). The *CO* mRNA profile simulated by model 2b lacked the *FKF1*-dependent shoulder at the end of the long photoperiod (Figure 3B), whereas model 1b had matched the *FT* mRNA based on data that included this shoulder. We therefore expected that using the simulated *CO* mRNA profile in model 3 would yield lower levels of simulated *FT* mRNA, compared to model 1b. A *CO* mRNA profile similar to an *fkf1* mutant might simply have yielded the low levels of *FT* mRNA that had been observed in *fkf1* mutant plants. The peak level of simulated *FT* mRNA in model 3 was indeed lower than observed in wild-type plants but, surprisingly, the reduction was only 40% (Figure 3D), which was an overestimate of an order of magnitude compared to the *FT* RNA levels observed in the *fkf1* mutant. Thus model 3 simulated a *CO* mRNA profile similar to the *fkf1* mutant but greatly overestimated the *FT* mRNA level. Removing *FKF1* in the mutant plant caused a much more severe reduction of *FT* mRNA levels than could be predicted from the effect of the *fkf1* mutation on *CO* mRNA levels alone. Consistent with this, adding the FKF1-dependent shoulder to the *CO* mRNA profile in preliminary model 3F1 had predicted only a modest increase in *FT* mRNA levels (Figure S4). Together, these results indicated that a major effect of *FKF1* may be to activate *FT* expression downstream or independently of *CO* mRNA.

To estimate the importance of *FKF1*-dependent activation for *FT* transcription, we constructed a speculative model (model 3F2), in which the observed FKF1 protein profile and the simulated CO protein together promoted *FT* transcription (see supplementary text). The model was matched to the training data sets (8 and 9; see Table S1) that allowed direct comparison of wild-type and *fkf1* mutant results (Figure 4). The new *CO* mRNA profiles were matched to the data for wild-type and *fkf1* mutant plants under long photoperiods, including the *FKF1*-dependent shoulder in the wild-type (Figures 4C and 4E). The model predicted a smaller effect of *FKF1* on *CO* RNA under short photoperiods, consistent with the data (Figure 4B). Simulated *FT* mRNA levels showed an improved profile in wild-type (Figure 4E). The aberrant morning peak of earlier models (Figures 2B and 2D) was removed, because FKF1 levels are low at dawn (Figure S4a). Simulations with model 3F2 showed that 90% of wild-type *FT* transcription at the end of a long photoperiod was FKF1-dependent.

The photoperiod-dependence of this effect was similar to the effect of FKF1 on *CO* transcription. This raised the possibility that CO and FKF1 cooperate to regulate both *CO* and *FT* transcription by a single mechanism, which would include a positive feedback of CO protein upon *CO* mRNA abundance (Figure 4J). To test this hypothesis, the FKF1-dependent shoulder of *CO* mRNA under long photoperiods was measured in wild-type plants and in seven mutant lines carrying *co* alleles that severely affect flowering time (Figure S7). Control *fkf1* mutant plants showed low *CO* mRNA levels 13h after dawn (about 25% of wild-type levels), consistent with Figure 4. *CO* mRNA was undetectable in one insertional mutant *co* allele. The other six alleles had *CO* mRNA levels very close to wild-type, showing that CO protein function was not required for the FKF1-dependent shoulder in *CO* transcription. These data favor the model depicted in Figure 4A, in which FKF1 has two distinct effects: its known regulation of *CO* mRNA levels, which does not require CO protein, and a previously-undescribed effect on *FT* expression, which depends on CO.

We next explored the qualitative patterns of *FT* regulation in response to a range of different light-dark cycles. As the FKF1 protein profiles required for model 3F2 were available for only two conditions, these simulations used model 3. *FT* mRNA levels increased in a non-linear fashion when the system was stably entrained to 24 hr light-dark cycles with longer photoperiods (Figure 5A). Treating a short-day-entrained system with one longer photoperiod had a more graded effect (Figure S5), indicating that circadian entrainment significantly affected the photoperiod response (see Discussion). Data to inform the component models were only available for a limited range of conditions, so it was not unexpected that the clock model did not entrain stably to some exotic light-dark cycles. The model remained strongly rhythmic in these conditions but phase variations between successive cycles indicated that it was not following a stable, entrained limit cycle, which was the condition imposed for our analysis (see Supplemental Data). Nonetheless, two patterns of *FT* regulation appeared physiologically relevant (Figure 5A). First, light-dark cycles of longer or shorter duration than 24 hr partially activated *FT* under all photoperiods and, second, the steepest increase of *FT* expression with photoperiod occurred under 24 hr cycles. Thus the model predicts that there will be an optimal cycle duration to obtain the strongest photoperiodic switch, likely in a 24 hr environment.

Model 4: Prediction of Flowering Time

Published flowering time data differ widely among *Arabidopsis* accessions and across laboratories, reflecting the many

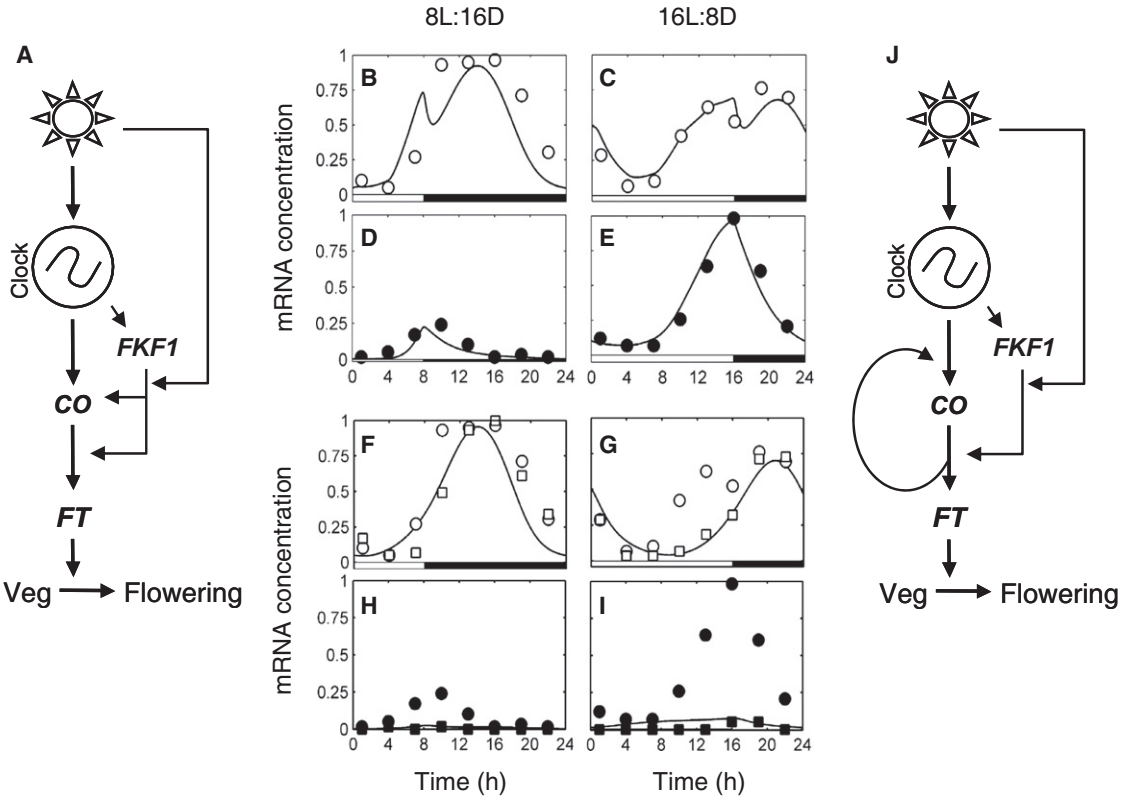

Figure 4. *FKF1* Affects *FT* Activation

Speculative model 3F2 (A) includes light-dependent activation of both *CO* and *FT* by *FKF1*. Simulations (solid lines) can closely match the expression patterns (Imaizumi et al., 2003) of *CO* (B, C, F, and G) and *FT* (D, E, H, and I) mRNA in both the wild-type (B–E) and *fkf1* mutant (F–I) under short-day (B, D, F, and H) and long-day (C, E, G, and I) conditions. An alternative, more parsimonious hypothesis is shown in (J): *FKF1* has a single effect on CO protein activity, which both controls *FT* transcription and feeds back positively to regulate *CO* transcription (see Figure S7). Open symbols, *CO* mRNA data; filled symbols, *FT* mRNA data; circles, data from wild-type; squares, data from *fkf1* mutant. Filled bar on time axis, dark interval; open bar, light interval.

environmental inputs that control absolute flowering time (Boss et al., 2004). Most molecular studies, moreover, have focused on one standard long and short photoperiod condition, so the non-linear relationship between the *FT* mRNA profile and flowering time could not be estimated from the data available (see supplementary text). We therefore compared flowering time data to the *FT* expression profiles predicted by model 3, where we could perform simulations for any photoperiod. Simple mathematical functions fitted well to flowering data for plants of the Columbia accession (Corbesier et al., 1996), with clear differences in the functions required for different experimental protocols (seeSupplemental Data, and Figure S6). A sigmoid function matched data sets from three laboratories that used similar experimental protocols: data on days to flowering in plants of the Columbia accession (Figure S6a, Corbesier et al., 1996) and data on total leaf numbers for plants of the Landsberg(*erecta*) accession (Figure 5B, Wilczek et al., 2009) and the Wassilewskija accession (Figure 5C, Pouteau et al., 2008). The critical photoperiod that elicited the half-maximal flowering response was almost identical in Figures 5B and 5C, despite the differences in absolute leaf numbers (see supplementary information). Mutation of *CO* prevents *FT* expression in the models, so *co* mutant plants are predicted to flower under all photoperiods with the same, high leaf number as wild-type plants under very short photoperiods, as confirmed in the recent data (Wilczek et al., 2009). The flowering function offers a standard approach to reveal robust behavior of the photoperiod response system.

DISCUSSION

The external coincidence model can clearly provide a workable photoperiod sensor (Carré et al., 2006). We aimed for a more detailed, quantitative explanation of the observed molecular regulation that could be linked to the whole-organism response. Our approach will be validated if the resulting models accurately predict the molecular data yet remain comprehensible, if the models direct future experimentation to address gaps in current data, and if the models give insight into comparable processes in other contexts. The data required need not present technical challenges. Consistent data sets for *CO* and *FT* mRNA levels and flowering times would already be valuable to explore a wider range of environmental conditions and genotypes with the full range of *FT* profiles, from *ft* mutants to *FT*-overexpressing lines. These data would test the simple functions assumed here for CO

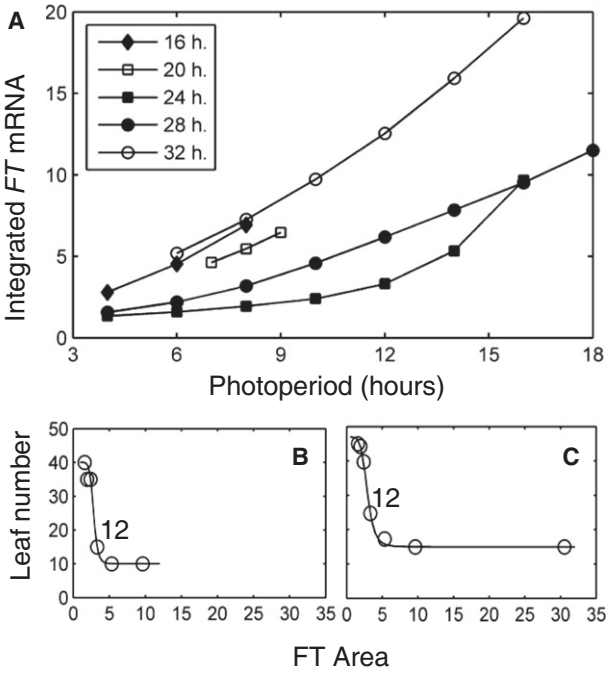

Figure 5. A Photoperiod Sensor for 24 hr Days, Regulating Flowering

(A) *FT* expression was simulated under light-dark cycles comprising 6–16 hr photoperiod in a total cycle duration of 16 hr (diamonds) to 32 hr (open circles), using model 3. 24 hr cycles show the largest ratio of integrated *FT* mRNA between long and short photoperiods. Absent results are due to unstable circadian entrainment in some conditions. (B and C) The integrated *FT* mRNA area simulated by model 3 under different photoperiods (diamonds) is related to flowering time data for the same photoperiods by a simple function (line), with specific parameter values (see Supplemental Data) for data sets from Landsberg(*erecta*) (B, Wilczek et al., 2009) and Wassilewskija (C, Pouteau et al., 2008). Flowering time data covered photoperiods from 6L:18D to 16L:8D in (B) and (C), with an additional data point for constant light in (C). The data point for 12L:12D is labeled (12).

protein synthesis and for the effectiveness of FT as a floral inducer. Current data were sufficient to make eight specific, testable predictions (Table S2), which are discussed below, together with their functional implications for photoperiod responses.

Suppressed Induction of *FT* in the Morning

A good overall fit after parameter optimization shows that a model is consistent with the molecular data. The simplest models of *FT* activation by light and *CO* were largely sufficient to recapitulate the molecular data. Simulating data from the *toc1* mutant confirmed that this mutation in the circadian clock affected *FT* regulation largely by altering rhythmic *CO* mRNA expression (Niwa et al., 2007; Yanovsky and Kay, 2002), though a small (~40%) increase in *FT* activation by another mechanism remains possible (prediction 2, Table S2). A specific failure of the model can be more informative. For example, the overestimation of *FT* levels at the start of a long photoperiod (Figure 2) suggested that another level of regulation reduces the effectiveness of *CO* at this time (prediction 1 in Supplemental Data). A similar, morning-specific suppression has been identified in experimental studies of *CO*-overexpressing plants (Valverde et al., 2004) and linked to phyB in *cop1* mutant plants (Jang et al., 2008). Our models show that this mechanism operates in wild-type plants, quantify its effects, show that the effect is greater in long than in short photoperiods (Figure S3), and suggest a molecular mechanism (Figure 4; see below). The quantitative effect of the suppression was modest (~60% reduction in *FT* activation in Figure S3) and its parameters were not well constrained, because it only affected one to two data points in the *FT* profile. Moreover, morning expression of *FT* can sometimes be observed experimentally (Corbesier et al., 2007), and flowering can be accelerated under exotic light cycles that drive high *CO* expression in the morning (Roden et al., 2002). Thus the morning suppression mechanism is not always effective at the level of *FT* expression and is not always relevant at the level of flowering time, though it is apparent in most of the molecular data sets considered here. Regulation by *FKF1* provides a parsimonious mechanism for the suppressive effect, as detailed below.

Regulation of *CO* by a Photoperiod-Responsive Clock

The circadian peak of *CO* RNA accumulation moves to a later phase under long photoperiods (Figure 2). The interlocking, dual feed-back loop model of the clock was required to match this phase delay (Figure 3, prediction 3 in supplemental table), because the phase of this clock model responds strongly to light at dusk (Locke et al., 2006). A more complex, three-loop clock model (Locke et al., 2006) matches better to data for circadian-regulated genes other than *CO*, where peak phase is much less delayed under long photoperiods (unpublished data; Millar and Kay, 1996). The *CO* entrainment profile is consistent with the two-loop model and therefore might reflect a distinct circadian clock mechanism that is restricted to specific cell types, for example in the vasculature (An et al., 2004). Circadian clocks with distinct entrainment patterns have also been proposed in the photoperiod sensor of the short-day plant, *Ipomoea nil* (Hayama et al., 2007). The unknown mechanism that regulates some aspects of the *CO* waveform independently of the *GI* rhythm (Fornara et al., 2009) might also be consistent with the unusual photoperiod-sensitivity of the timing of peak *CO* RNA.

The dusk-sensitive entrainment of *CO* makes the system more responsive to lengthening photoperiods, particularly to delays in lights-off, than it is to stable, long photoperiods. The sensitivity to photoperiod change arises because the first lengthened photoperiod simply allows a longer duration of light to coincide with a *CO* mRNA rhythm that is set to the early phase characteristic of a short day, as proposed by Bünning's external coincidence mechanism (Bünning, 1936). Under stable, long photoperiods, however, the observed phase of the *CO* rhythm is delayed, moving more of the *CO* mRNA peak into the dark interval. After entrainment to 8 hr photoperiods, for example, model 3 predicted a significantly greater *FT* area on the first 10 hr or 12 hr photoperiod than it did when stably entrained to 10 hr or 12 hr photoperiods (Figure S5). The circadian entrainment of *CO* is consistent with observed flowering responses to changes in the time of sunset, which have evolved exquisite sensitivity in tropical trees (Borchert et al., 2005).

Regulation of *CO* and *FT* by *FKF1* and Photoperiod

Whereas circadian entrainment delays *CO* expression under longer photoperiods, *FKF1* promotes earlier *CO* mRNA accumulation (reviewed in Imaizumi and Kay, 2006). The *FKF1*-dependent shoulder in *CO* RNA accumulation was readily simulated by adding a second source of *CO* RNA to supplement the waveform driven only by the clock model (Figures 3, 4, and S4). This source could be either an arbitrary square waveform (data not shown) or the observed FKF1 protein profile, which also has a sharp onset and decline (Imaizumi et al., 2003). In either case, the sharp change in the additional *CO* was important to match the dip in *CO* RNA profile that is often observed at the end of a long photoperiod (prediction 5).

Our models (Figures 3 and 4) highlighted a dramatic and previously unsuspected effect of *FKF1,* to promote *FT* expression independently of its effect on *CO* RNA accumulation (prediction 6). For an intuitive illustration, consider that the levels of *CO* mRNA in the light are comparable or higher in *fkf1* mutants under long photoperiods compared to the wild-type under short photoperiods (compare Figure 3B with 3A), yet the cognate *FT* mRNA levels are much lower in the mutants (Figures 3C and 3D). Direct interaction of FKF1 with CO protein might enhance CO function (Fukamatsu et al., 2005), providing a mechanism based on known components. Light-stabilized CO protein would then activate *FT* transcription in an FKF1-dependent manner. This was achieved in a revised model by using the FKF1 protein profile to drive the transcription of *FT* in addition to its effect on *CO* (model 3F2, see Supplemental Data). This speculative model matched wild-type *FT* mRNA waveforms well and lacked the morning-specific peak of FT expression observed with earlier models (Figure 4). As *FKF1* is not expressed in the morning, simulated *FT* mRNA expression remains low at this time even if *CO* RNA is present. Thus the postulated function of *FKF1* provides a parsimonious molecular mechanism for the morning "gate" (prediction 1). Constitutive expression of *FKF1* and *GI* was insufficient to activate *FT* expression immediately after dawn (Sawa et al., 2007), however, indicating that further analysis of the morning "gate" is warranted. FKF1 was estimated to increase *FT* transcription 10-fold in our model compared to the *fkf1* mutant, highlighting the importance of FKF1 as a photoperiodic regulator (Imaizumi and Kay, 2006). FKF1 increased *CO* transcription by only 35%, suggesting that FKF1-independent factors are also important in regulating *CO* mRNA levels (Fornara et al., 2009; Imaizumi et al., 2005).

The relationship between the two effects of *FKF1*, on *CO* and *FT*, is unclear. A possible extension to model 3F2 was to propose that FKF1 functioned together with CO protein, and that this mechanism activated both *FT* and *CO* transcription (prediction 7). This parsimonious hypothesis predicted that CO protein would be required for the *FKF1*-dependent shoulder of *CO* mRNA under long photoperiods. New experimental data for the *CO* mRNA levels of seven *co* mutant alleles failed to support this notion (Figure S7). Our results therefore predict that *FKF1* functions differently to regulate *CO* and *FT*, indicating that a novel regulatory mechanism is involved in the control of *FT*. It is possible that this function is *GI*-dependent, as *GI* regulates flowering via the circadian expression of *CO* (as in our models) but also by a genetically-separable mechanism (Gould et al., 2006; Mizoguchi et al., 2005).

Tuning the Mechanisms of Day-Length Perception

The circadian clock models entrained stably to a limited range of exotic light-dark cycles with total durations that varied from 24 hr (Figure 5). The models were developed using data from only constant conditions and 12L:12D cycles (Locke et al., 2005a; Locke et al., 2005b), so more flexible models might be constructed based upon new data on the clock components under other conditions. The mathematical theory of coupled oscillators (Guckenheimer and Holmes, 1983) shows that stable entrainment occurs when the system parameters are within an area of parameter space described as the Arnold tongue. Changing the period of the entraining cycle significantly away from the period of the oscillator moves the system outside the Arnold tongue. Consistent with theory, the clock model then becomes quasi-periodic, as also reported for circadian rhythms in many species.

Using model simulations, we predicted that discrimination between long and short light intervals will be greatest when the total duration of the entraining cycle is 24 hr (Figure 5; prediction 8). This qualitative prediction is reminiscent of the classic experiments on soybean (Hamner and Takimoto, 1964) and matches more detailed data from the hamster, where photoperiodic regulation of the reproductive system also showed the greatest amplitude under 24 hr cycles (Elliott, 1974). This effect also can be related to the theory of coupled oscillators (Guckenheimer and Holmes, 1983). Altering the duration of the entraining cycle by a moderate amount relative to the period of the oscillator moves the system within the Arnold tongue, and alters the phases of the clock components. The circadian clock is presumed to be adapted to the 24 hr entraining cycles in which it has evolved: the clock components (and outputs such as *CO*) will be regulated with peak phases that are physiologically optimal (Pittendrigh and Daan, 1976). Changing the duration of the entraining cycle will alter their phases and lead to a suboptimal response, either slowing growth (Dodd et al., 2005), or in this case weakening the photoperiodic sensor.

Our models illustrate how the external coincidence mechanism has evolved in *Arabidopsis* to a more elaborate form than Bünning's original hypothesis. CO protein was the first molecular correlate of photoperiod to be identified and its dual regulation by the clock (transcriptionally) and by light (post-translationally) forms an external coincidence detector. The photoperiod-sensitive entrainment of the *CO* mRNA rhythm extends beyond the simplest external coincidence hypothesis and has potential functional significance in detecting photoperiod change, but may require specialized circadian timing, as discussed above. FKF1 forms a second external coincidence detector that regulates *CO* mRNA (Imaizumi et al., 2003) and we show that it is crucial in activating *FT* (prediction 6). As CO and FKF1 function together to regulate *FT* at the end of the photoperiod, separating their expression in time might in principle be sufficient to prevent flower induction under short photoperiods, as proposed by the internal coincidence hypothesis (Pittendrigh, 1960). It will be interesting to determine whether the entrainment of their circadian rhythms (and the rhythms of other clock-controlled

regulators) responds differently to photoperiods, as this would be required to introduce an aspect of internal coincidence (as implied in Imaizumi and Kay, 2006). In contrast, another photoperiodic mechanism appears to control the degradation rate of cry2 protein at the start of the day (El-Din El-Assal et al., 2001). The effect of cry2 degradation on photoperiodism is unclear, and our current models match *FT* mRNA profiles without this modulation of light input.

The existence of multiple photoperiod sensors has important consequences for understanding plant physiology. First, it greatly increases the potential for specialized photoperiodic sensors to control different physiological responses within a single species, including responses of vegetative organs. Second, it is unclear which (or how many) of the molecular mechanisms will be conserved across species with similar photoperiodic responses. Finally, it increases the possibility that species with different photoperiodic responses might differ radically in their molecular mechanisms. It is therefore all the more striking that homologs of *CO* and *FT* have been implicated in the short-day photoperiodic response of the dicots *Ipomoea nil* (Hayama et al., 2007) and poplar (Bohlenius et al., 2006) and of the monocot rice (the genes Hd1 and Hd3a, respectively, reviewed in Hayama and Coupland, 2004; Izawa, 2007). The profile of *Hd1* RNA strongly resembles that of *CO* (Figure S8a), such that Hayama et al. (Hayama et al., 2003) proposed that a single change of sign, equivalent to making *CO* a negative regulator of *FT*, would be sufficient to convert the long-day response of *Arabidopsis* to the short-day response of rice. Using RNA profiles of *Hd1* and *Hd3a* under long and short photoperiods, we constructed the simplest model of the rice photoperiod sensor based upon our *Arabidopsis* models (see supplemental data). The proposed repressive function of *Hd1* could fully account for the photoperiodic regulation of the mean level of *Hd3a*, because the coincidence of light with *Hd1* RNA in the evening changes significantly between long and short photoperiods. There is, however, little or no difference in *Hd3a* expression in the evening, so coincidence does not directly explain the temporal profile. Peak *Hd3a* expression occurs in the morning (Figure S8b), and matching this timing required a separate (and unknown) clock-regulated factor distinct from the *Hd1* repressor. It will be interesting to determine how the morning-specific photoperiodic regulator of *Hd3a* relates to the well-described, evening-specific regulators in *Arabidopsis*. There are now several possible candidates in rice (reviewed in Hayama and Coupland, 2004; Izawa, 2007). Recent data give this added relevance for *Arabidopsis*, because *FT* can also be expressed in the morning in some conditions (Corbesier et al., 2007), suggesting that the rice regulatory mechanism might also be present in *Arabidopsis*.

The photoperiodic switch is part of a broader network of developmental pathways and environmental responses that control the flowering of *Arabidopsis* (Boss et al., 2004). Models of this broad network (Welch et al., 2003) have the exciting potential to link our detailed molecular mechanisms to larger-scale phenological models. These already have widespread applications in crop scheduling and crop improvement (Adams et al., 2001; Hammer et al., 2006) and have been successfully applied to *Arabidopsis* development (Wilczek et al., 2009).

EXPERIMENTAL PROCEDURES

Plant Growth and RNA Assays

Seeds of *fkf1*, the *co* alleles and cognate wild-types were generously supplied by G. Coupland (Koeln) or by the Nottingham *Arabidopsis* Stock Centre. Plants were grown as described (Locke et al., 2005b) under 16L:8D for 10 days at 22°C. Samples were harvested 13h after lights-on; RNA was extracted and analyzed by qRT-PCR as described (Locke et al., 2005b).

Computational Methods

Quantitative expression profiles for *CO* and *FT* mRNA under various conditions were digitized from charts or graphs in the literature or kindly provided by the original authors (see Supplemental Data). Timeseries data were numbered (see Table S1), normalized and checked for consistency (see Supplemental Data). Twenty-eight timeseries from wild-type plants were used for most model training and validation, with ten further timeseries from *toc1* and *fkf1* mutants. Models were constructed as ordinary differential equations in Matlab (Mathworks, Cambridge UK); SBML versions will be available from the Biomodels repository upon publication (Le Novere et al., 2006), and in versions compatible with the Circadian Modeling simulation interface (available at www.amillar.org/Downloads.htm). Model equations and parameters are presented in the supplemental data. Parameters were estimated by fitting to the relevant data (for the wild-type, to the training data sets 1, 3, 8, and 9; see Table S1), using a boundary value solver to ensure that the model produced stable, limit cycle solutions (see supplemental data). Models 3F1 and 3F2 including FKF1 function are described as speculative, because there is much less quantitative timeseries data available for FKF1 in the literature than for *CO* and *FT*. We test these models only in 8L:16D and 16L:8D conditions, where FKF1 data are available.

SUPPLEMENTAL DATA

Supplemental Data include Supplemental Experimental Procedures, Supplemental References, two tables, and eight figures and can be found with this article online at http://www.cell.com/supplemental/S0092-8674(09)01487-1.

ACKNOWLEDGMENTS

A.J.M. gratefully acknowledges discussions with Carl Johnson, Steve Welch, and Peter Crawford; seed stocks provided by George Coupland; and the hospitality of Luis Serrano and the Centre de Regulació Genòmica, Barcelona during revision of the manuscript. J.D.S. and T.S. performed modeling studies; J.F. performed experimental work; P.E.B. and J.C.W.L. provided modeling tools; J.D.S., T.S., I.A.C., D.A.R. and A.J.M. designed modeling studies; K.J.H. and A.J.M. designed experimental work; A.J.M. wrote the paper with comments from all authors. This work was supported by BBSRC award BEP17427 to A.J.M., D.A.R. and I.A.C., and by BBSRC/EPSRC SABR award F0052371 to K.J.H., A.J.M., D.A.R. and others. J.C.W.L. was supported by a Sainsbury Postgraduate Scholarship from the Gatsby Charitable Trust. T.S. was supported by a Postgraduate Scholarship from the Royal Thai Government. D.A.R. holds an EPSRC Senior Fellowship and is supported by EU BioSim Network Contract 005137. The Centre for Systems Biology at Edinburgh is a Centre for Integrative Systems Biology supported by BBSRC and EPSRC award D019621.

Received: February 7, 2009
Revised: July 13, 2009
Accepted: November 17, 2009
Published: December 10, 2009

REFERENCES

Adams, S.R., Pearson, S., and Hadley, P. (2001). Improving quantitative flowering models through a better understanding of the phases of photoperiod sensitivity. J. Exp. Bot. *52*, 655–662.

An, H., Roussot, C., Suarez-Lopez, P., Corbesier, L., Vincent, C., Pineiro, M., Hepworth, S., Mouradov, A., Justin, S., Turnbull, C., and Coupland, G. (2004). CONSTANS acts in the phloem to regulate a systemic signal that induces photoperiodic flowering of Arabidopsis. Development *131*, 3615–3626.

Bohlenius, H., Huang, T., Charbonnel-Campaa, L., Brunner, A.M., Jansson, S., Strauss, S.H., and Nilsson, O. (2006). CO/FT regulatory module controls timing of flowering and seasonal growth cessation in trees. Science *312*, 1040–1043.

Borchert, R., Renner, S.S., Calle, Z., Navarrete, D., Tye, A., Gautier, L., Spichiger, R., and von Hildebrand, P. (2005). Photoperiodic induction of synchronous flowering near the Equator. Nature *433*, 627–629.

Boss, P.K., Bastow, R.M., Mylne, J.S., and Dean, C. (2004). Multiple pathways in the decision to flower: enabling, promoting, and resetting. Plant Cell *16* (*Suppl*), S18–S31.

Bünning, E. (1936). Die Endogene Tagesrhythmik als Grundlage der Photoperiodischen Reaktion. Ber. Dtsch. Bot. Ges. *54*, 590–607.

Carré, I.A., Coupland, G., and Putterill, J. (2006). Photoperiodic responses and the regulation of flowering. In Endogenous Plant Rhythms, A. Hall and H.G. McWatters, eds., pp. 167–190.

Corbesier, L., Gadisseur, I., Silvestre, G., Jacqmard, A., and Bernier, G. (1996). Design in *Arabidopsis thaliana* of a synchronous system of floral induction by one long day. Plant J. *9*, 947–952.

Corbesier, L., Vincent, C., Jang, S., Fornara, F., Fan, Q., Searle, I., Giakountis, A., Farrona, S., Gissot, L., Turnbull, C., and Coupland, G. (2007). FT protein movement contributes to long-distance signaling in floral induction of Arabidopsis. Science *316*, 1030–1033.

Dodd, A.N., Salathia, N., Hall, A., Kevei, E., Toth, R., Nagy, F., Hibberd, J.M., Millar, A.J., and Webb, A.A. (2005). Plant circadian clocks increase photosynthesis, growth, survival, and competitive advantage. Science *309*, 630–633.

El-Din El-Assal, S., Alonso-Blanco, C., Peeters, A.J., Raz, V., and Koornneef, M. (2001). A QTL for flowering time in Arabidopsis reveals a novel allele of CRY2. Nat. Genet. *29*, 435–440.

Elliott, J.A. (1974). Photoperiodic regulation of testis function in the golden hamster: Relation to the Circadian System (Austin, TX: University of Texas).

Fornara, F., Panigrahi, K.C., Gissot, L., Sauerbrunn, N., Ruhl, M., Jarillo, J.A., and Coupland, G. (2009). Arabidopsis DOF transcription factors act redundantly to reduce CONSTANS expression and are essential for a photoperiodic flowering response. Dev. Cell *17*, 75–86.

Fukamatsu, Y., Mitsui, S., Yasuhara, M., Tokioka, Y., Ihara, N., Fujita, S., and Kiyosue, T. (2005). Identification of LOV KELCH PROTEIN2 (LKP2)-Interacting Factors that Can Recruit LKP2 to Nuclear Bodies. Plant Cell Physiol. *46*, 1340–1349.

Gould, P.D., Locke, J.C., Larue, C., Southern, M.M., Davis, S.J., Hanano, S., Moyle, R., Milich, R., Putterill, J., Millar, A.J., and Hall, A. (2006). The molecular basis of temperature compensation in the Arabidopsis circadian clock. Plant Cell *18*, 1177–1187.

Guckenheimer, J., and Holmes, P. (1983). Nonlinear Oscillations, Dynamical Systems and Bifurcations of Vector Fields (New York: Springer Verlag).

Hammer, G., Cooper, M., Tardieu, F., Welch, S., Walsh, B., van Eeuwijk, F., Chapman, S., and Podlich, D. (2006). Models for navigating biological complexity in breeding improved crop plants. Trends Plant Sci. *11*, 587–593.

Hamner, K.C., and Takimoto, A. (1964). Circadian Rhythms and Plant Photoperiodism. Am. Nat. *98*, 295–322.

Hayama, R., Agashe, B., Luley, E., King, R., and Coupland, G. (2007). A circadian rhythm set by dusk determines the expression of FT homologs and the short-day photoperiodic flowering response in Pharbitis. Plant Cell *19*, 2988–3000.

Hayama, R., and Coupland, G. (2004). The molecular basis of diversity in the photoperiodic flowering responses of Arabidopsis and rice. Plant Physiol. *135*, 677–684.

Hayama, R., Yokoi, S., Tamaki, S., Yano, M., and Shimamoto, K. (2003). Adaptation of photoperiodic control pathways produces short-day flowering in rice. Nature *422*, 719–722.

Hazlerigg, D., and Loudon, A. (2008). New insights into ancient seasonal life timers. Curr. Biol. *18*, R795–R804.

Imaizumi, T., and Kay, S.A. (2006). Photoperiodic control of flowering: not only by coincidence. Trends Plant Sci. *11*, 550–558.

Imaizumi, T., Schultz, T.F., Harmon, F.G., Ho, L.A., and Kay, S.A. (2005). FKF1 F-box protein mediates cyclic degradation of a repressor of CONSTANS in Arabidopsis. Science *309*, 293–297.

Imaizumi, T., Tran, H.G., Swartz, T.E., Briggs, W.R., and Kay, S.A. (2003). FKF1 is essential for photoperiodic-specific light signalling in Arabidopsis. Nature *426*, 302–306.

Izawa, T. (2007). Daylength measurements by rice plants in photoperiodic short-day flowering. Int. Rev. Cytol. *256*, 191–222.

Jang, S., Marchal, V., Panigrahi, K.C., Wenkel, S., Soppe, W., Deng, X.W., Valverde, F., and Coupland, G. (2008). Arabidopsis COP1 shapes the temporal pattern of CO accumulation conferring a photoperiodic flowering response. EMBO J. *27*, 1277–1288.

Kobayashi, Y., and Weigel, D. (2007). Move on up, it's time for change–mobile signals controlling photoperiod-dependent flowering. Genes Dev. *21*, 2371–2384.

Le Novere, N., Bornstein, B., Broicher, A., Courtot, M., Donizelli, M., Dharuri, H., Li, L., Sauro, H., Schilstra, M., Shapiro, B., et al. (2006). BioModels Database: a free, centralized database of curated, published, quantitative kinetic models of biochemical and cellular systems. Nucleic Acids Res. *34*, D689–D691.

Locke, J.C., Kozma-Bognar, L., Gould, P.D., Feher, B., Kevei, E., Nagy, F., Turner, M.S., Hall, A., and Millar, A.J. (2006). Experimental validation of a predicted feedback loop in the multi-oscillator clock of Arabidopsis thaliana. Mol. Syst. Biol. *2*, 59.

Locke, J.C., Millar, A.J., and Turner, M.S. (2005a). Modelling genetic networks with noisy and varied experimental data: the circadian clock in Arabidopsis thaliana. J. Theor. Biol. *234*, 383–393.

Locke, J.C., Southern, M.M., Kozma-Bognar, L., Hibberd, V., Brown, P.E., Turner, M.S., and Millar, A.J. (2005b). Extension of a genetic network model by iterative experimentation and mathematical analysis. Mol. Syst. Biol. *1*, 13.

Millar, A.J., and Kay, S.A. (1996). Integration of circadian and phototransduction pathways in the network controlling *CAB* gene transcription in Arabidopsis. Proc. Natl. Acad. Sci. USA *93*, 15491–15496.

Mizoguchi, T., Wright, L., Fujiwara, S., Cremer, F., Lee, K., Onouchi, H., Mouradov, A., Fowler, S., Kamada, H., Putterill, J., and Coupland, G. (2005). Distinct roles of GIGANTEA in promoting flowering and regulating circadian rhythms in Arabidopsis. Plant Cell *17*, 2255–2270.

Niwa, Y., Ito, S., Nakamichi, N., Mizoguchi, T., Niinuma, K., Yamashino, T., and Mizuno, T. (2007). Genetic linkages of the circadian clock-associated genes, TOC1, CCA1 and LHY, in the photoperiodic control of flowering time in Arabidopsis thaliana. Plant Cell Physiol. *48*, 925–937.

Oosterom, E. Hammer, G., and Chapman, S. (2004). Can transition to flowering be modelled dynamically from the gene level? In 4th International Crop Science Congress (Brisbane, Australia).

Pittendrigh, C.S. (1960). Circadian rhythms and the circadian organisation of living systems. Cold Spring Harb. Symp. Quant. Biol. *25*, 159–184.

Pittendrigh, C.S., and Daan, S. (1976). A functional analysis of circadian pacemakers in nocturnal rodents. V. A clock for all seasons. J. Comp. Physiol. [A] *106*, 333–355.

Pouteau, S., Carre, I., Gaudin, V., Ferret, V., Lefebvre, D., and Wilson, M. (2008). Diversification of photoperiodic response patterns in a collection of early-flowering mutants of Arabidopsis. Plant Physiol. *148*, 1465–1473.

Roden, L.C., Song, H.R., Jackson, S., Morris, K., and Carre, I.A. (2002). Floral responses to photoperiod are correlated with the timing of rhythmic expression relative to dawn and dusk in Arabidopsis. Proc. Natl. Acad. Sci. USA *99*, 13313–13318.

Sawa, M., Nusinow, D.A., Kay, S.A., and Imaizumi, T. (2007). FKF1 and GIGANTEA complex formation is required for day-length measurement in Arabidopsis. Science *318*, 261–265.

Suarez-Lopez, P., Wheatley, K., Robson, F., Onouchi, H., Valverde, F., and Coupland, G. (2001). CONSTANS mediates between the circadian clock and the control of flowering in Arabidopsis. Nature *410*, 1116–1120.

Thomas, B., and Vince-Prue, D. (1997). Photoperiodism in plants (San Diego, CA: Academic Press).

Turck, F., Fornara, F., and Coupland, G. (2008). Regulation and Identity of Florigen: FLOWERING LOCUS T Moves Center Stage. Annu. Rev. Plant Biol. *59*, 573–594.

Valverde, F., Mouradov, A., Soppe, W., Ravenscroft, D., Samach, A., and Coupland, G. (2004). Photoreceptor regulation of CONSTANS protein in photoperiodic flowering. Science *303*, 1003–1006.

Welch, S.M., Roe, J.L., and Dong, Z.S. (2003). A genetic neural network model of flowering time control in Arabidopsis thaliana. Agron. J. *95*, 71–81.

Wilczek, A.M., Roe, J.L., Knapp, M.C., Cooper, M.D., Lopez-Gallego, C., Martin, L.J., Muir, C.D., Sim, S., Walker, A., Anderson, J., et al. (2009). Effects of genetic perturbation on seasonal life history plasticity. Science *323*, 930–934.

Yanovsky, M.J., and Kay, S.A. (2002). Molecular basis of seasonal time measurement in Arabidopsis. Nature *419*, 308–312.

Cell, Volume *139*

Supplemental Data

Prediction of Photoperiodic Regulators from Quantitative Gene Circuit Models

José Domingo Salazar, Treenut Saithong, Paul E. Brown, Julia Foreman, James C.W. Locke, Karen J. Halliday, Isabelle A. Carré, David A. Rand, and Andrew J. Millar

Figure S1

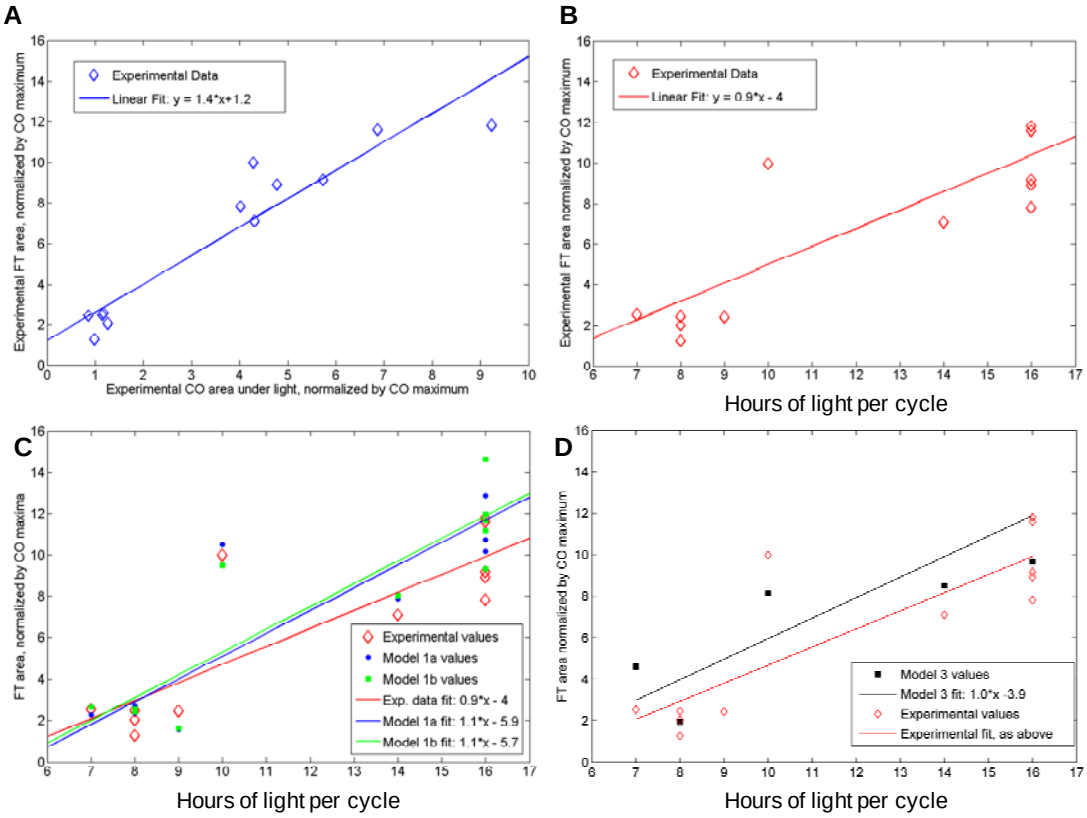

Figure S2

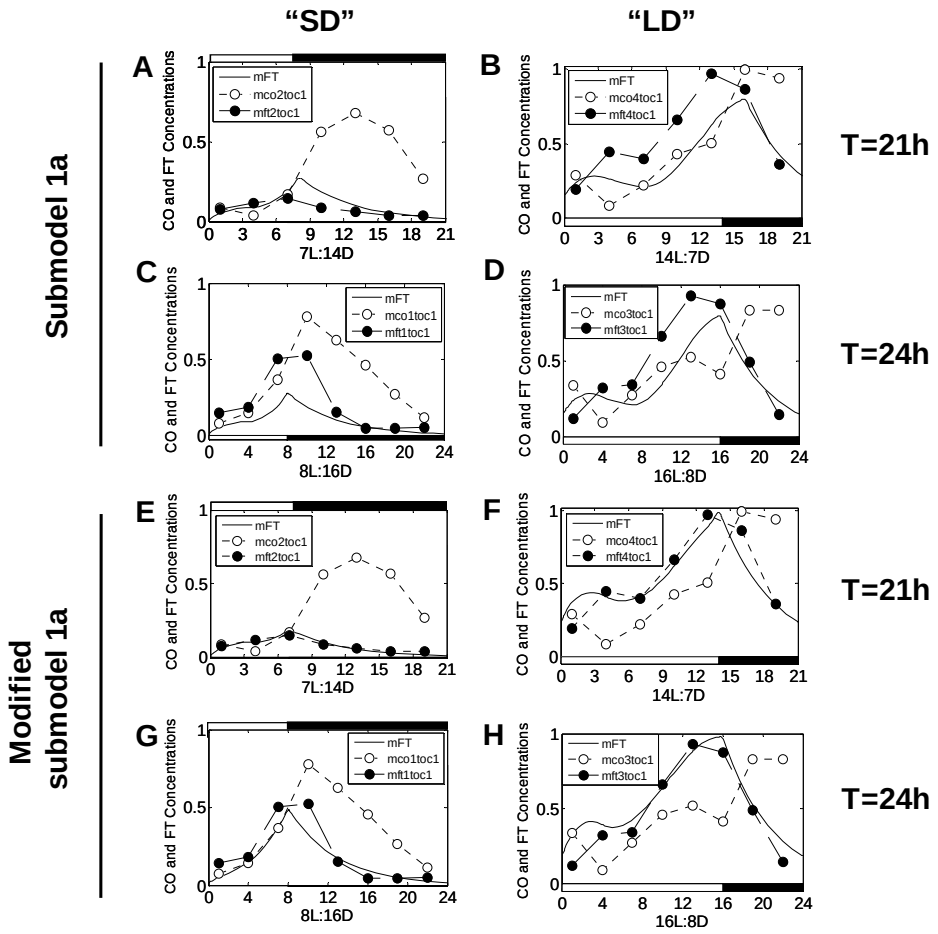
"SD"
"LD"
Submodel 1a
Modified submodel 1a
A
B
C
D
E
F
G
H
mFT
mco2toc1
mft2toc1
mco4toc1
mft4toc1
mco1toc1
mft1toc1
mco3toc1
mft3toc1
CO and FT Concentrations
7L:14D
14L:7D
8L:16D
16L:8D
T=21h
T=24h

Figure S3

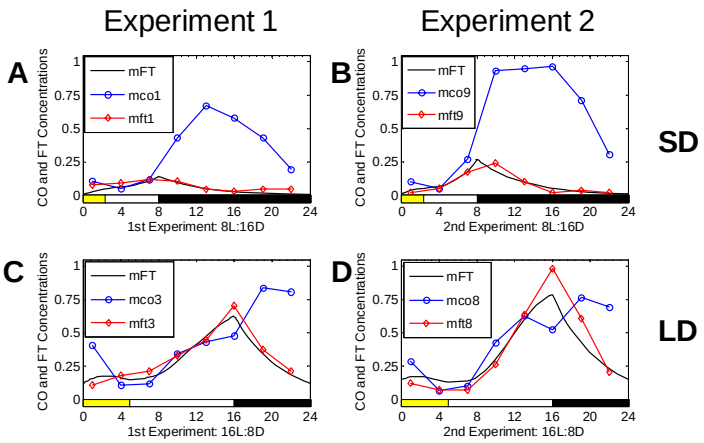
Experiment 1
Experiment 2
A
B
C
D
SD
LD
CO and FT Concentrations
mFT
mco1
mft1
mco9
mft9
mco3
mft3
mco8
mft8
1st Experiment: 8L:16D
2nd Experiment: 8L:16D
1st Experiment: 16L:8D
2nd Experiment: 16L:8D

Figure S4

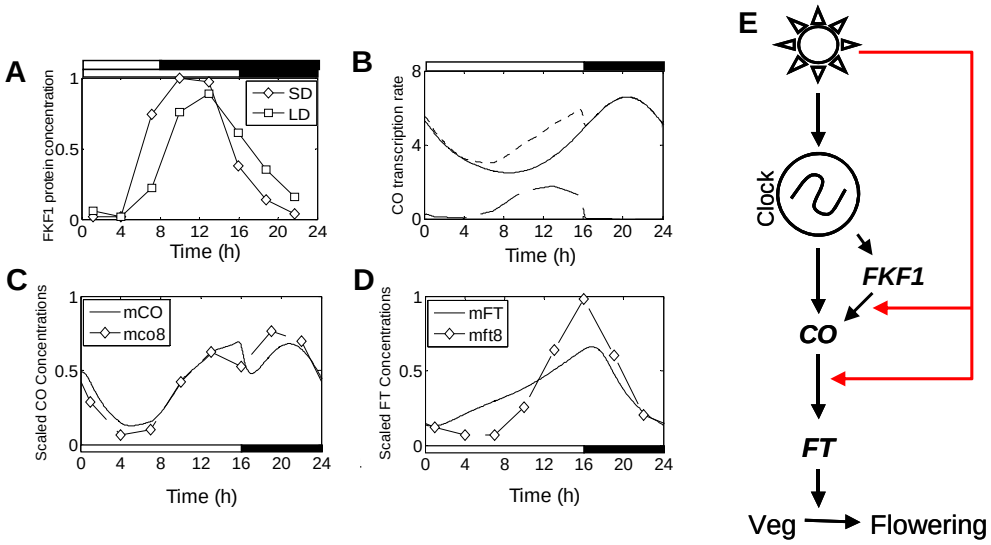
A
FKF1 protein concentration
SD
LD
Time (h)
B
CO transcription rate
Time (h)
C
Scaled CO Concentrations
mCO
mco8
Time (h)
D
Scaled FT Concentrations
mFT
mft8
Time (h)
E
Clock
FKF1
CO
FT
Veg
Flowering

Figure S5

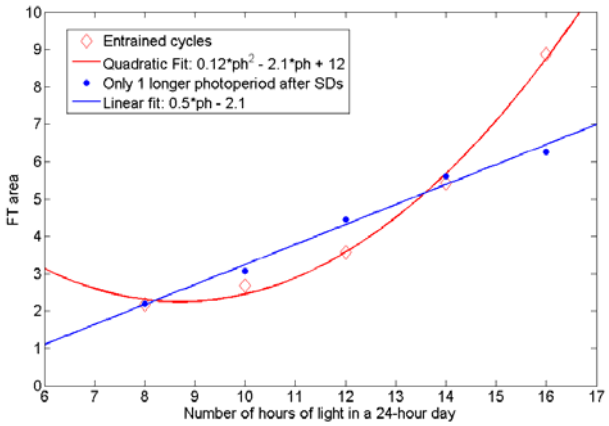
Entrained cycles
Quadratic Fit: 0.12*ph^2 - 2.1*ph + 12
Only 1 longer photoperiod after SDs
Linear fit: 0.5*ph - 2.1
FT area
Number of hours of light in a 24-hour day
0
1
2
3
4
5
6
7
8
9
10
6
7
8
9
10
11
12
13
14
15
16
17

Figure S6

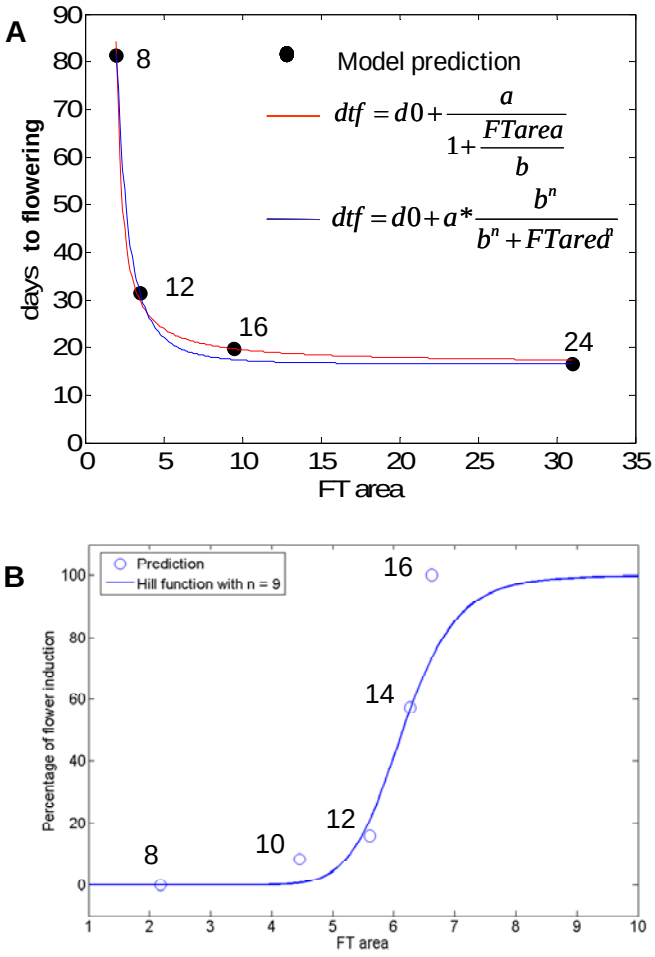
A
days to flowering
FT area
Model prediction
$dtf = d0 + \frac{a}{1 + \frac{FTarea}{b}}$
$dtf = d0 + a * \frac{b^n}{b^n + FTared^n}$
8
12
16
24
B
Prediction
Hill function with n = 9
Percentage of flower induction
FT area
8
10
12
14
16

Figure S7

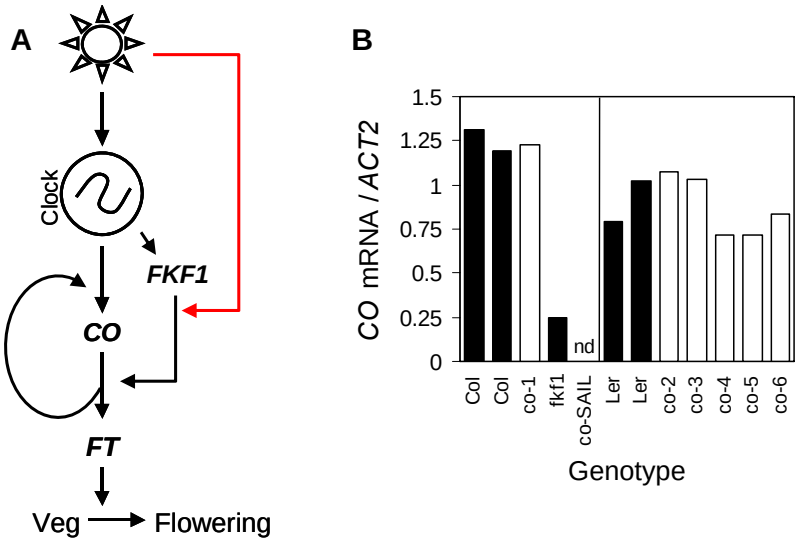
A
Clock
FKF1
CO
FT
Veg
Flowering
B
CO mRNA / ACT2
1.5
1.25
1
0.75
0.5
0.25
0
nd
Col
Col
co-1
fkf1
co-SAIL
Ler
Ler
co-2
co-3
co-4
co-5
co-6
Genotype

Figure S8

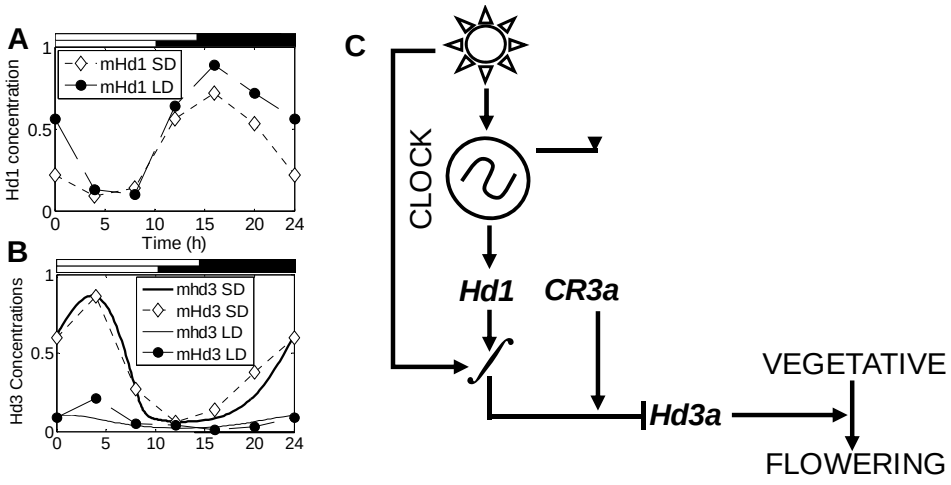
A
Hd1 concentration
mHd1 SD
mHd1 LD
Time (h)
B
Hd3 Concentrations
mhd3 SD
mHd3 SD
mhd3 LD
mHd3 LD
C
CLOCK
Hd1
CR3a
Hd3a
VEGETATIVE
FLOWERING

Supplemental figure legends

Figure S1. Molecular data from several laboratories conform to the external coincidence hypothesis.

The validation data (see Supplemental Data; Supplemental Table 1) were analysed to identify the trends across all experiments. (A) The integrated *FT* mRNA area over one cycle is strongly correlated with the integrated *CO* mRNA area during the light interval. (B) the integrated *FT* mRNA area over one cycle is more flexibly related to the hours of light during the cycle. The experimental mRNA levels have been normalized to the *CO* mRNA maximum (see Supplemental data). (C) Simulations of models 1a (blue symbols) and 1b (green symbols) optimized using the training data were then compared to the validation data of (B). (D) Simulations of model 3 (black symbols) were compared to the validation data of (B). In each case, solid lines show a linear fit to the cognate data series, indicating the overall trend of the data or simulations.

Figure S2. The *toc1* mutation has little effect on light activation of *FT.*

Data redrawn from (Yanovsky and Kay, 2002) depict mRNA levels of *CO* (open symbols) and *FT* (filled symbols) in the *toc1-1* mutant under light:dark cycles of 21h (A, B, E, F, T=21h) or 24h (C, D, G, H, T=24h). In each case, short (A, C, E, G) and long (B, D, F, H) photoperiod conditions are shown. The simulated *FT* mRNA levels (solid line) are shown, from simulations using model 1a with parameters optimised for the wild type (a-d) or model 1a with parameter *Vco* altered to match the *toc1* data sets, changing from 26 nmol/h in wild type to 37 (E, F) or to 35 (G, H).

Figure S3. *CO* activates less *FT* expression in the early morning.

The over-activation of *FT* mRNA in model 1a (Figure 2) was estimated by reducing the effectiveness of light in activating *FT* in the morning. Best-fit parameters for the duration and extent of this morning gate were estimated by fitting simulations (solid lines) based on observed *CO* mRNA levels (blue circles) to observed *FT* mRNA levels (red diamonds) from the two training data sets (Imaizumi et al., 2003; Yanovsky and Kay, 2002), under SD (A, B) and LD (C, D). The effects shown for SD are duration 2.3 h, effective light intensity 60% of normal; and for LD, duration 5 h, intensity 40% of normal.

Figure S4. Simulating the effect of FKF1 on *CO* expression.
(A) Accumulation patterns of FKF1 protein under 8L:16D ('SD') and 16L:8D ('LD'), redrawn from Imaizumi *et al* (2003). (B) The additional *CO* transcription due to FKF1 activation under 16L:8D is plotted alone (dashed line) and superimposed (dotted line) upon the original rate of *CO* transcription from model 3 (solid line). The mRNA expression patterns for *CO* (C) and *FT* (D) were simulated by model 3F1 including the activation of *CO* by FKF1 protein (solid lines), with the corresponding experimental data (diamonds). (E) depicts the circuit originally proposed by Imaizumi *et al.* (2003).

Figure S5. Entrainment of the circadian clock contributes to the photoperiod switch. Model 3 was stably entrained to 24h cycles with various photoperiods, as in Figure 1 of Corbesier *et al*. (1996). The *FT* mRNA area integrated over 24h of simulation is shown (open diamonds, with quadratic fit). Alternatively, *FT* mRNA area was measured following transfer from 8L:16D short photoperiods to a single test

photoperiod of the duration shown (filled circles, with linear fit), as in Figure 3 of Corbesier *et al*., (1996).

Figure S6. Effective relationships between the predicted *FT* area and flowering time in the Columbia accession.

The *FT* areas predicted in Supplemental figure 5 are plotted against the flowering time data of Corbesier *et al*. (1996), Figure 1 (a) and Figure 3 (b). The relationships are described by two effective functions (A, see legend), or by a sigmoid function (B). Parameter values are given in the Supplemental data, equations (11) - (13). Figures beside each data point show the cognate photoperiod (h).

Figure S7. Functional CO protein is not required to produce the *FKF1*-dependent shoulder of *CO* mRNA in long photoperiods.

(A) Hypothetical circuit, in which the dual effects of *FKF1* on *CO* and *FT* mRNA are accomplished by a single molecular function of FKF1 at the level of CO protein. CO protein is proposed to feed back to regulate the shoulder of *CO* mRNA. Under this model, mutation of *CO* should prevent the FKF1-dependent activation of *CO* transcription in long photoperiods.

(B) Seedlings with and without *co* mutations were grown under 16L:8D for 10 days at 22°C. Samples were harvested 13h after lights-on, and extracted RNA was analysed by qRT-PCR. The *fkf1* mutant strongly reduces *CO* mRNA expression at this time, but *co* mutations have little or no effect. Filled bars, wild types and *fkf1* mutant control. Col, Columbia parent; Ler, Landsberg *erecta* parent. Open bars, *co* mutant alleles. The *co-SAIL* allele is line SAIL_24_H04 and lacks *CO* mRNA due to a T-DNA insertion (nd, not detectable).

Figure S8. The molecular photoperiod response in rice.

mRNA expression profiles are shown for the *CO* homologue *Hd1* (A) and the *FT* homologue *Hd3a* (B), under 10L:14D (open symbols, SD) and 14L:10D (filled symbols, LD), from (Hayama et al., 2003). Simulated Hd3a expression is shown under SD (bold solid line) and under LD (solid line). C shows the hypothetical circuit, in which the coincidence of light with *Hd1* expression is integrated ($\int$) before it inhibits expression of *Hd3a*. A hypothetical circadian regulator (CR3a) controls the timing of *Hd3a* expression during the diurnal cycle. *Hd3a* promotes flowering, as *FT* does in Arabidopsis.

Supplemental Experimental Procedures

Data Collection and Analysis

Numerical values for *CO* and *FT* mRNA expression patterns were captured by digitising published charts or graphs of quantified data, or were kindly provided by the original authors (Supplemental Table 1). Experiments are numbered; pairs of *CO* and *FT* waveforms collected in the same genotype and experiment are given the same number. The data include some variation in experimental details but share a similar basic design. In particular, wild-type plants under short photoperiods (8L:16D) and long photoperiods (16L:8D) were tested in 3 and 7 experiments, respectively, with more limited representation of exotic, non-24h cycles. Several Arabidopsis accessions were tested, as well as *fkf1* or *toc1* mutants and *CO*-overexpression lines. RNA levels were measured using RT-PCR in all cases, with detection either by real-time fluorescence labelling or by hybridisation of radio-labelled probes. The mRNA used as a constitutive control for inter-sample normalization varied. Primers that amplify *UBIQUITIN* (*UBQ*) transcripts (Blazquez and Weigel, 1999) were used in experiments 1-12 and similar primers (Cerdan and Chory, 2003) for experiments 13 and 14. Experiment 15 (Somers et al., 2004) used *ACTIN*2 (*ACT2*). In one experiment, the ratio *FT/CO* was quantified directly (Valverde et al., 2004).

As a preliminary comparison between experiments, the ratio of peak *FT* to *CO* levels was calculated to determine whether these different waveforms were mutually compatible (data not shown). There is potential for significant variation in some experimental methods, for example the specific radioactivity of the probes used in the hybridization experiments might vary as a function of their age. The ratio (peak *FT* / peak *CO*) fell in a range 0.13 to 1.3, with the exception of experiments 11 (ratio = 3.3), where radiolabelling was used, and 15 (ratio = 6.4), possibly related to the *ACT2* control. Waveform 12 had by some distance the lowest ratio (0.15) of any experiment in a long photoperiod. The *FT* waveform ftcoox1 in the *CO*-

over-expression experiment of (Suarez-Lopez et al., 2001) lacks comparable information on the *CO* mRNA. In contrast, the other *FT* data from *CO*-over-expression lines, coox2 and coox3, are normalized to the level of *CO* mRNA (Valverde et al., 2004). For these reasons, the data of (Suarez-Lopez et al., 2001) and (Somers et al., 2004) were not considered further.

Data analysis and normalisation for modelling

The remaining data were tested for comparability. According to the simplest formulation of the external coincidence hypothesis in Arabidopsis, *FT* expression should be related to the integrated area under the curve of *CO* mRNA accumulation that coincides with light. The set of selected data was tested against this hypothesis, to confirm that pooling results from diverse sources did not obscure interpretation of the data. This entails comparisons across experiments that might use different experimental control transcripts for technical standardization. The data for all genes and photoperiods within each experiment were therefore normalized to a common internal standard, the maximum level of *CO* mRNA in wild-type plants under short (8L:16D) photoperiods. *CO* mRNA has a broad, flat-topped waveform in these conditions, which reduces the variability due to the particular timepoint chosen for sampling in different experiments. Integrated areas were calculated under the *CO* mRNA curve during the light interval only, and under the *FT* mRNA curve over a full cycle. The *FT* area is clearly positively correlated with the *CO* area that coincides with light, across all the data sets (supplemental figure 1A). Variation among experiments accounted for less than a 2-fold range in the FT areas under conditions that gave similar CO areas. As an additional test, the normalized *FT* area was plotted against the duration of light in each cycle (Supplemental figure 1B). The correlation was also positive but this result is weaker, because the available data are clustered around 8h light and 16h light with very little data at intermediate photoperiods. Futhermore, the variation in experimental conditions produces clear outliers, for example from experiment 6 (10L:20D).

To take account of some of the variability, two different short day (SD) and long day (LD) experiments were used in the initial estimation of the model parameters (the training data sets): experiments 1 and 9 (short photoperiods), 3 and 8 (long photoperiods). These were produced by the Kay laboratory (Imaizumi et al., 2003; Yanovsky and Kay, 2002), and allowed direct comparison between these wild-type waveforms used to develop the models and the *toc1* and *fkf1* mutant waveforms that were tested in the same experiments.

In order to compare model simulations to the experimental waveforms, the simulations were normalized to the maximum of *CO* mRNA under SD. Simulations were normalized by dividing the *CO* and *FT* waveforms in SD and LD by the maximum of the simulated *CO* waveform of the wild type in SD, then multiplying them by the maximum of the experimental *CO* waveform in SD. In this way, the simulated and experimental *CO* waveforms in SD share the same upper limit (Figure 3). This procedure is unnecessary for models 1a and 1b, which take their normalization directly from the size of the experimental *CO* waveform (Figure 2).

Model Testing Procedure

The kinetic parameters required in the model equations have not been directly measured by experiment. Random parameter sets (usually over 3,000, with each parameter usually bounded in the range 0 to 100) were therefore evaluated, by testing the fit of the model solution with that parameter set to the training data, using Matlab version 6 (Mathworks, Cambridge, UK). The model was solved for 120 hours (five 24-hour days) of entrainment under the appropriate light-dark cycle, with a final cycle that was used as the seed for a differential equation boundary value solver (bvp4c, MatLab version 6). The resulting solution was therefore guaranteed to be a true, attracting limit cycle. After using the scaling described in the previous paragraph, the fit of the model to the relevant data set(s) was measured using a weighted mean square method. The weights were chosen to be the maximum of the experimental CO and FT mRNA waveforms in each photocycle (short or long days) to

prevent the fitting procedure being dominated by the largest FT mRNA abundance in long days.

The 20 parameter sets with lowest cost (best fit) were typically subject to 5 cycles of 20 iterations of the Nelder-Mead unconstrained simplex optimization method (Matlab version 6)**.** The Nelder-Mead method typically improved the cost values by 20-30%, frequently changing the cost ranking compared to the starting parameter sets. After optimization, the difference in cost values of the 20 best solutions tended to be small, although some parameter values could be widely spread in parameter space.

Models

Our models are based on Michaelis-Menten kinetics. All parameter values are positive, so terms that model the degradation of the relevant molecular species are given negative sign. In the equations below, the term L = 1 for light and 0 for darkness. The square waveform of light:dark cycles in growth chamber experiments was simulated using a hyperbolic tangent function to produce abrupt light-dark transitions that are numerically continuous. Throughout, units of time are hours (h); characteristic units for molecular species are nanomoles (nmol); the relative mRNA profiles were normalized to an internal mRNA standard as noted below.

For a diagrammatic representation of the different models and their relationships, see Figure 1.

Level 1 – Regulation of *FT* by the *CO* concentration observed in data

Model 1a

FT mRNA synthesis is a function of the experimental *CO* mRNA amount, which is taken to approximate the amount of active CO protein. *CO* activates *FT* transcription only in the light (equation 1).

$$\frac{dmFT}{dt} = L \cdot vCO \cdot \frac{eCO}{kCO + eCO} - vFT \frac{mFT}{kFT + mFT} \quad (1)$$

mFT = simulated *FT* mRNA, vCO = maximum FT transcription rate = 25.9719 nmol/h, kCO = Michaelis constant of *FT* activation by CO = 70.6788 nmol, eCO = experimental *CO* mRNA concentration, vFT = max rate of *FT* mRNA degradation = 12.9543 nmol/h, kFT = Michaelis constant of *FT* mRNA degradation = 62.2131 nmol.

Model 1b

The experimental *CO* mRNA amount is translated into CO protein that is degraded only in darkness (2). CO protein activates *FT* transcription equally in all conditions (3).

$$\frac{dCOp}{dt} = vCOm \cdot eCO - (1 - L) \cdot vCOp \frac{COp}{kCOp + COp} \quad (2)$$

COp = simulated CO protein, $vCOm$ = rate constant of CO protein production = 3.3243 nmol/h, eCO = *CO* mRNA concentration in experimental data, $vCOp$ = maximum rate of CO protein degradation = 10.4291 nmol/h, $kCOp$ = Michaelis constant of CO protein degradation = 1.4977 nmol.

$$\frac{dmFT}{dt} = vCOFT \frac{COp}{kCOFT + COp} - vFT \frac{mFT}{kFT + mFT} \quad (3)$$

$vCOFT$ = max *FT* transcription rate = 0.4561 nmol/h, $kCOFT$ = constant of activation by CO = 9.9181 nmol, vFT = max rate of *FT* mRNA degradation = 4.9569 nmol/h and kFT = Michaelis constant of *FT* mRNA degradation = 12.3926 nmol.

Either model 1a or 1b could fit well to the experimental data (Supplemental Figure 1C). As model 1b explicitly includes regulation of the CO protein, we anticipate that this will be more useful for comparison to molecular data, and discuss the results from this model in the main text.

The "morning gate"

To reduce the excess *FT* mRNA predicted in the morning (Figure 2), we inserted new parameters into model 1a that reduced the effectiveness of light in activating *FT* (by multiplying *vCO* by a constant value between 0 and 1), for a specified time interval (between 0 and 6 hours) starting at dawn. No single combination of effectiveness and duration parameters allowed an improved fit to the training data under both long days and short days (unpublished results). The data could only be matched by allowing the gating parameters to vary with photoperiod. A good fit was obtained for some parameter sets with no gating at all under short-day conditions. The best fits resulted from a lower gating effect (and/or for a shorter interval) under short photoperiods, combined with stronger gating (and/or for a longer interval) under long photoperiods (Supplemental figure 3 and legend shows one example). The morning gate improved the fit to only one to two data points in the available *FT* RNA timeseries, making a relatively small contribution to the overall fit. By the same token, the time resolution of the current data provides insufficient constraints to parameterise the effect accurately. Moreover, several experimental results indicate that the gate is not always effective at the molecular level, nor functionally relevant for flowering (see Discussion). No separate morning gate mechanism was included in subsequent models.

Level 2 – Regulation of *CO* mRNA by the circadian clock

Model 2a

This model is based on the first clock model (Locke et al., 2005a), which consists of two genes, *LHY* and *TOC1*, that form a single negative feedback loop. Light entrains the clock model only by enhancing *LHY* transcription, so the phase of the clock is locked to lights-on.

The nuclear TOC1 protein concentration from this model peaks at an appropriate phase under short days, and is therefore used without modification as a proxy for *CO* mRNA.

Model 2b

This model is based on the interlocking-loop clock model (Locke et al., 2005b). This clock model consists of four genes *LHY*, *TOC1* and two unknown genes termed *X* and *Y*, in which *LHY, TOC1,* and *X* form one loop, while *TOC1* interacts with *Y* to form a second, interlocking feedback loop. Light activates transcription of *LHY* and also of *Y.* Again, the nuclear TOC1 protein concentration is used as a proxy for *CO* mRNA.

As model 2a clearly failed to fit the phase change relative to lights-on that was observed in the experimental *CO* data (Figure 2), only model 2b was used subsequently.

Level 3 – Regulation of *FT* by simulated *CO*

Model 3

This model combines *CO* simulated using model 2b with the activation of *FT* mRNA simulated using model 1b (equations 2 and 3). Neither model is modified but *nTOC1* replaces *eCO* in equation (2):

$$\frac{dCOp}{dt} = vCOm \cdot nTOC1 - (1 - L) \cdot vCOp \frac{COp}{kCOp + COp} \qquad (4)$$

Parameter values are the same as in (2). *nTOC1* = nuclear TOC1 protein.

Modelling FKF1 effects on *CO* and *FT* transcription

Preliminary models were constructed to quantify the effects of *FKF1* upon *CO* and *FT* mRNA profiles. A simple step function gave a good qualitative fit to the shoulder of *CO* mRNA at the end of a long photoperiod (data not shown). As FKF1 protein profiles were quantified by Imaizumi *et al*. (2003) (Supplemental figure 4A), we modelled a more detailed molecular mechanism using these data for 8L:16D and 16L:8D cycles. Our aim here was to fit the *CO*

mRNA waveform in the wild-type plants of one data set as closely as possible, in order to distinguish quantitatively between a possible direct effect of FKF1 on *FT,* compared to an indirect effect of FKF1 on *FT* transcription *via* the regulation of *CO*.

Model 3F1 - FKF1 activation of CO *mRNA*

The profile of simulated *CO* mRNA from model 2b (mCO_{TOC1}, originally nuclear TOC1 protein) was modified to fit training data set 8 rather than all four training data sets (Supplemental figure 4B, 4C). As the measured *CO* mRNA in this data set was greater than the simulated value during the light interval (Figure 3B), a negative term corresponding to a *CO* mRNA degradation rate was slightly increased (by 0.04% of its original value) during the light interval. All other parameters remained as in model 2b. The increase in *CO* mRNA due to FKF1 was included as an additional source of *CO* mRNA (mCO_{FKF1}) using a simple, linear equation (5, see Supplemental figure 4B). The transcription rate is linearly dependent on the observed FKF1 protein level ($FKF1$) and is active only during the light interval, when L = 1.

$$\frac{dmCO_{FKF1}}{dt} = L \cdot vCO_{FKF1} \cdot FKF1 - vFKF \cdot mCO_{FKF1} \qquad (5)$$

$vCOFKF1$ = transcriptional activation rate by FKF1 (2 nmol/h), $vFKF$ = mRNA degradation rate (1.8674 nmol/h).

Total *CO* mRNA ($mCO_{TOC1} + mCO_{FKF1}$) closely matched the observed *CO* mRNA profile of data set 8. The additional source of *CO* mRNA briefly increased the simulated wild-type *CO* mRNA profile at the end of the short photoperiod (Figure 4B), consistent with the slight reduction in *CO* mRNA at this time in *fkf1* mutants compared to wild-type plants (Figure 4B). Translating this pool produced CO protein as in (2), and the resulting CO protein activated *FT* as in (3). Under long photoperiods, the increased *CO* mRNA level yielded higher peak *FT* mRNA levels (Supplemental figure 4D), giving a slightly improved match to the *FT* data at 16h compared with the simulation using model 3 (compare with Figure 3D). This effect on *FT* in the wild-type simulation would scarcely justify including the increased complexity of *CO* mRNA regulation but simulations of the *fkf1* mutant were more revealing. In model 3F1, the

FT transcription rate at the end of a long photoperiod (16h after dawn) was only 35% lower in the simulated *fkf1* mutant compared to wild type.

Model 3F2 - Speculative model for FKF1 activation of FT *mRNA*

The level of *FT* mRNA observed in *fkf1* mutant plants (Figure 3D) was far lower than the prediction from model 3, which lacked *FKF1* (Figure 3D), leading us to speculate that FKF1 was also required to activate *FT* transcription. We modified equation (3) to include the activation of *FT* transcription by FKF1 protein in the light, giving equation (6), with results shown in Figure 4A. FKF1 activation of *FT* was implemented as a multiplicative term in (6), because the effect of the *fkf1* mutation on *FT* mRNA levels was much more severe than its effect on *CO* mRNA. A large proportion of *FT* mRNA thus becomes *FKF1*-dependent. For parsimony, we assumed FKF1 was equally effective in regulating *CO* and *FT*. Parameter $vCOFT$ was altered compared to (3) to account for the new regulator. New parameters B_{CO} and B_{FKF} were added in order to estimate CO-independent and FKF1-independent *FT* transcription rates, respectively. These were termed 'basal' transcription rates to indicate that their regulation is unknown, not that it is necessarily unregulated.

$$\frac{dmFT}{dt} = \left(B_{CO} + vCOFT \cdot \frac{COp}{kCOFT + COp} \right) \cdot \left(B_{FKF} + L \cdot vCOFKF1 \cdot FKF1 \right) - vFT \cdot \frac{mFT}{kFT + mFT}$$

(6)

$vCOFT$ = max CO-dependent *FT* transcription rate = 0.58 nmol/h, $kCOFT$ = constant of activation by CO = 9.9181 nmol, B_{CO} = CO-independent transcription rate = 0 nmol/h, B_{FKF} = FKF1-independent transcription rate = 0.22 nmol/h, $vCOFKF1$ = coupling constant for activation by FKF1 = 2 nmol/h, vFT = mRNA degradation rate = 1.8674 nmol/h, kFT = Michaelis constant of *FT* mRNA degradation = 5.3925 nmol.

With B_{CO} set to 0, *FT* transcription remains completely *CO*-dependent, consistent with undetectable *FT* levels in the *co* mutant (Jang et al., 2008; Suarez-Lopez et al., 2001). The parameter is included in the model to reflect the possibility that a small proportion of *FT*

expression is CO-independent in wild-type plants. Simulations (data not shown) suggested that the upper bound on the parameter value consistent with experimentally undetectable *FT* mRNA (~5% of wild-type peak level) in the *co* mutant is about 0.03 (data not shown), 7-fold less than B_{FKF} and 19-fold less than $vCOFT$. As the numerical value of this very low transcription rate was arbitrary, and it had a negligible effect on *FT* in wild-type simulations (data not shown), it was set to 0 for parsimony. Future experiments that reliably quantify the low levels of *FT* RNA in the *co* mutant may constrain its value above zero.

In order to simulate the *fkf1* mutant, the parameter controlling FKF1's transcriptional effect ($vCOFKF1$) was set to 0 in (5) and (6). The simulated *CO* mRNA profiles (Figure 4F, 4G) were very close to the simulations from model 3, as expected. Reduced *CO* mRNA and protein remained, allowing us to estimate the basal transcription rate of *FT* that was required to produce the small amounts of *FT* mRNA observed in the experimental data on the *fkf1* mutant (Figures 4H, 4I). The net transcription rate at the end of a 16h day was 0.0522 nmol/h in the mutant, compared to 0.5317 nmol/h in wild type. This result emphasizes the large effect of the *fkf1* mutation on *FT* expression, which greatly exceeds the effect expected from the change in *CO* mRNA alone (illustrated by model 3F1, above).

Level 4 – Regulation of flowering time by *FT*

In the final stage of modeling, a direct predictor of flowering time was added to the model. This requires one of the model outputs to be connected to a measure of macroscopic flowering time that corresponds to experimental data (the percentage of plants flowering on a given day, the mean time (days) until flowering or the duration of the vegetative phase (number of leaves) until flowering). There was no suitable data in the literature to define directly the non-linear relationship between the amount of *FT* mRNA and the time to flowering. Such data cannot easily be pooled, as flowering times are highly variable between laboratories and even between experiments. Rather, both variables must be measured for a range of photoperiods in a single experiment. Such data are now urgently required.

In the interim, photoperiod was used as an intermediate variable between the model outputs and the experimental measures of flowering. The level 3 models take photoperiod as an input parameter, so it was possible to predict the relationship between any of the model components and photoperiod. All the flowering measures in the literature are also reported as a function of photoperiod. The level 4 model can therefore be used to interpolate the flowering time for any photoperiod by calibrating the predicted *FT* against the measured flowering times.

Mathematically speaking, if *fl*(*ph*) is an experimental measure of flowering *fl* (for example, leaf number) in a photoperiod *ph*, and *Q* refers to a molecular quantity (*FT* mRNA concentration, for example), then flowering *fl* under photoperiod *ph* is a function of *Q* under photoperiod *ph*. This relationship is defined by function *X* (in our example, *X* is relationship of leaf number to *FT* mRNA concentration), thus:

$$fl(ph) = X(Q(ph)). \quad (7)$$

As *fl(ph)* is known experimentally and our molecular models will give us an approximation to *Q(ph)*, which we will call *Q*(ph)*, then we can compute an approximation to *X* (termed *X**) using measured *fl(ph)* values from the literature:

$$fl(ph) = X^*(Q^*(ph)). \quad (8)$$

Using *X** we can obtain by interpolation an approximation to *fl(ph), fl*(ph),* for other photoperiods that have not been measured:

$$fl^*(ph) = X^*(Q^*(ph)). \quad (9)$$

We analysed flowering-time data of Corbesier *et al*. (Corbesier et al., 1996), which offers several useful data sets, by this method to illustrate the approach. The data include flowering time (as “days to macroscopic appearance of flower buds”) of non-vernalized Columbia plants under various photoperiods (in figure 1 of the paper), and flowering time (as “percentage of [plants showing] flower induction”) of vernalized Columbia plants maintained

in SD for 2 months then treated with a single test cycle of various photoperiods (in figure 3a of the paper).

In order to compute *Q*(ph)* for the conditions used in Figure 1, model 3b was entrained to light:dark cycles with various photoperiods and *FT* mRNA area was calculated (the area beneath the curve of *FT* mRNA level integrated over a 24h cycle). Thus the full model provides *Q*(ph)* in a complex form. The same relationship between *FT* area and photoperiod can be more simply approximated by a quadratic function (see Supplemental figure 5), given by

$$FTarea = 0.12ph^2 - 2.1ph + 12. \quad (10)$$

The data point for a 24h photoperiod (constant light) also fits the quadratic relationship well.

X(Q*(ph))* could be computed in several ways, depending on the data. The measured flowering times in Figure 1 of (Corbesier et al., 1996) exhibit a switching behavior when plotted against either photoperiod or *FT* area, which can be approximated by a sigmoid function. The change in flowering time is greatest between 8h photoperiod (>80 days to flowering) and 12h photoperiod (~30 days), where predicted *FT* area is low and changes relatively little (supplemental figure 6A). The leftmost point is therefore in a region of very steep gradient, where flowering times change quickly for even a slight change in *FT* area. It is unclear where the flowering times will saturate, and in practice growth rates may be markedly reduced under very short photoperiods owing to metabolic effects. No saturating sigmoid function was found to match these data as well as a non-saturating function, given by

$$\text{Flowering time} = d0 + a / (1 - FTarea/b) \quad (11)$$

where *d0* is a minimum flowering time at very high *FTarea* (estimated at 16.55 days), *a* is a multiplier (estimated at -15.29), *FTarea* is as described above and *b* is an artificial lower limit of *FT* area that prevents flowering completely (estimated value 1.63). Supplemental figure 6A shows this function plotted together with the most closely-matching Hill function,

$$Data = d1 + a1\frac{b1^n}{b1^n + FTarea^n} \quad (12)$$

with parameter values a1 = 662.081, b1 = 0.93871, n = 1 and d1 = 16.5 days. In this function, d1 is again the minimum flowering time, a1 is a multiplier, b1 is the *FTarea* at the so-called “critical photoperiod”, and n is the Hill coefficient. The critical photoperiod is conventionally defined as the photoperiod that causes the half-maximal flowering response, between the fully-induced and fully-uninduced conditions. Higher Hill coefficients allow a sharper switch from the uninduced to the induced response, over a narrower range of *FTarea*. Because this data set did not include sufficiently short photoperiods to indicate the maximum flowering time, the limits of the response were unclear: the Hill coefficient was set to 1 and the value of b1 was also poorly constrained.

Data sets that include a greater range of photoperiods can show that the flowering response is minimally induced at short photoperiods and is saturated at long photoperiods. The Hill function (12) is equally applicable to data for flowering time (days to flowering) and for leaf numbers, as high leaf numbers at flowering reflect late flowering time. Equation (12) can therefore match the leaf number data of Pouteau *et al.* for the Ws accession (Pouteau et al., 2008) and the leaf number data of Wilczek *et al.* for the La(*er*) accession (Wilczek et al., 2009). For Wilczek et al. (Figure 5B), best-fit parameter values are n = 10, d1 = 10, a1 = 30.0669 and b1 = 2.82065. For Pouteau *et al.* (Figure 5C), best-fit parameter values are n = 6, d1 = 15, a1 = 31.9573 and b1 = 2.88922. In these cases, d1 is the minimum leaf number observed with fully-induced flowering, which is lower in the La(*er*) data than in Ws. Note the high values of n, which confer switching behaviour, and the very similar estimates of *b1*, which reflect similar critical photoperiods in both data sets.

Equation (12) can be directly related to the photoperiod submodel in the recent phenological model for Arabidopsis (Wilczek et al., 2009). Parameter d1 corresponds to the reciprocal of the developmental rate for photoperiods below the critical short day length. The upper and

lower turning points on either side of the critical day length correspond to the FTarea at the critical long and short day length (Wilczek et al., 2009), respectively.

In order to compute *Q*(ph)* for the conditions used in Figure 3 of (Corbesier et al., 1996), model 3b was entrained to SD (8L:16D) cycles and then tested under one longer photoperiod. Within the single, test photoperiod the model exhibited little change in mCO waveform compared to the preceding SD conditions (data not shown), because the entrainment of the clock was hardly affected within the first photoperiod. The mFT waveform was changed by the longer light intervals, resulting in a steep linear increase in the FT area (Supplemental figure 5). Note that this contrasts with the quadratic increase observed for the simulations under continuous cycles of altered photoperiod, where the entrainment of the clock also varies with the photoperiod (Supplemental figure 5; see Discussion).

X(Q*(ph))* was fitted with a sigmoid function, assuming that flowering was maximally induced by a 20L:4D cycle :

$$\%\,Flowering\,Induction = k1\frac{\left(FT\,area - FTarea(SD)\right)^n}{P\_crit^n + \left(FT\,area - FTarea(SD)\right)^n} + k0 \qquad (13)$$

where *k0* = 0, the % flowering in the SD control plants, *k1* = 100 for full induction, *P_crit* = 3.97 and the best value for *n* is probably 9. This represents a very steep switching behavior, very similar to what is observed in Figure 3(a) of (Corbesier et al., 1996) (Supplemental figure 6B).

Overall, this analysis supports the use of the *FT* area as a relevant model output for flowering prediction. Functions similar to (11), (12) and (13) above can readily be adapted to accommodate the variations in flowering time due to the growth conditions of specific laboratories, so that the model-based estimate, *X*(FTarea*(ph))*, can be used to interpret molecular data. Multiple data sets with matched FT areas and flowering times are now

required to define a measured *X(FTarea(ph))* function, in order to validate the model-based estimate and to assess the variations among laboratories.

Photoperiod responses over multiple cycles and transient changes in photoperiod

In order for the plant to integrate the *FT* over a full diurnal cycle, as *FTarea* does in the model, a moderately stable molecule may be required downstream of the *FT* mRNA. Levels of this integrating molecule would then cross a threshold for flowering upon a single long photoperiod, in the case of the SD-grown plants in Figure 3a of (Corbesier et al., 1996). The effective stability of the integrator must be limited, however, to ensure that the current or most recent photoperiods have the greatest effect. Excessive stability would allow long-term accumulation to induce flowering in plants held under SD conditions for 2 months without an inductive photoperiod, in contradiction to the data (Corbesier et al., 1996). Where young seedlings are tested (for example, Corbesier et al., 2007), several LD are required to induce flowering, indicating that the integrating species is stable enough to accumulate over several days. *FT* expression also increases progressively after each LD, and one cycle with high *FT* expression is observed after plants are returned from LD to SD (Corbesier et al., 2007). The latter effects are suggestive of a positive feedback in the photoperiod sensor. As the mechanism(s) of these effects remain to be determined, they are not included in the models presented.

Daylength perception in a short-day plant

A dramatic re-tuning of the photoperiod sensor is thought to have occurred in rice, to promote flowering in SD rather than LD (Hayama and Coupland, 2004). The *CO* orthologue of rice, *Heading date 1 (Hd1*), is expressed in a very similar fashion to Arabidopsis *CO* under both LD and SD (Supplemental figure 8A). Rather than activating expression of *FT* as in Arabidopsis, genetic evidence indicates that *Hd1* suppresses the best-characterised rice homologue of *FT*, named *Hd3a* (Hayama and Coupland). This change of sign has been proposed to account for the difference in mechanism between short-day plants and long-day

plants (Hayama et al., 2003). The published timeseries data for these rice genes are fewer and more variable than in Arabidopsis. Nonetheless, modeling of the rice data set that is most similar to Arabidopsis showed that, even for these data, the change of sign does not account for the dynamic expression pattern of *Hd3a* (data not shown). The same conclusion can be reached by inspection of the data (Supplemental figure 8B): light coincides with the highest *Hd1* RNA levels 12h after dawn under LD, but this peak of *Hd1* passes in darkness under SD. If light interacts with *Hd1* as it does with *CO*, this should result in differential induction of *Hd3a* in LD versus SD, yet *Hd3a* RNA levels at this time are almost identical in both conditions. Furthermore, about 4h after dawn *Hd1* expression falls to similar, low levels under LD and SD, yet this is when *Hd3a* RNA levels show the greatest photoperiodic regulation.

We propose that the coincidence of *Hd1* with light sets the mean level of *Hd3a* expression but that the phase of expression is set by another rhythmic factor, which we term the Circadian Regulator of *Hd3a* (CR3a). Activation of *Hd3a* transcription may for example require interaction between the Hd1 protein and a rhythmically expressed transcription factor. CR3a can be equally well approximated using a sine wave (Supplemental figure 8) or the waveform of *Hd1* RNA (unpublished results). CR3a can be modeled as either an activator or repressor of Hd3a, where activating CR3a peaks shortly after dawn (as in Supplemental figure 8) or repressive CR3a peaks early in the night (unpublished results).

$$\frac{dmHd3a}{dt} = B + vHd1 \cdot \frac{kHd1}{1 + \left(kHd1 + INT\right)} - vHd3a \cdot \frac{mHd3a}{kHd3a + mHd3a} + vCR3a \cdot \frac{CR3a}{kCR3a + CR3a} \quad (13)$$

$$CR3a = 1 + \cos\left(\frac{2\pi\left(t + \phi_{CR3a}\right)}{\tau_{CR3a}}\right) \quad (14)$$

B = basal level of *Hd3a* transcription (0.05 nmol/h), *vHd1* = maximum *Hd3a* transcription antagonized by Hd1 inhibition (2.545 nmol/h), *kHd1* = Michaelis constant of inhibition by Hd1 (2.3291 nmol), *INT* = measured integral of *Hd1* mRNA area during light interval over one 24h

cycle (1.39 nmol under 10L14D, 4.32 nmol under 14L10D), *vHd3a* = maximum rate of *Hd3a* mRNA degradation (1.9861 nmol/h), *kHd3a* = Michaelis constant of *Hd3a* degradation (0.0327 nmol), *vCR3a* = maximum *Hd3a* transcription rate from CR3a activation (4.4770 nmol/h), *kCR3a* = Michaelis constant of activation by *CR3a* (10.9056 nmol), Φ_{CR3a} = phase of *CR3a* transcription (-0.6242 h), τ_{CR3a} = period of *CR3a* transcription (24h).

Moreover, the relevant coincidence of *Hd1* with light cannot result in immediate regulation of *Hd3a*, nor can the coincidence be integrated uniformly within the day starting from dawn, as both mechanisms would predict the greatest difference in *Hd3a* expression at the end of the day. We therefore propose that the coincidence of *Hd1* RNA with light is integrated over longer time intervals spanning several days, and that this integrated measurement sets the mean level of *Hd3a* expression. The rice mechanism is therefore quite distinct from the very rapid effect in Arabidopsis of the coincidence of CO with light. Supplemental figure 8 shows that this class of mechanism readily fits the data. A parsimonious molecular mechanism is that Hd1 protein is much more stable than CO, accumulating over several days. A paralogue of CO that is rhythmically expressed with a peak near dawn (Kim et al., 2008), like CONSTANS-LIKE1 in Arabidopsis (Ledger et al., 2001), might function as an activating CR3a, though Hd1 is also proposed to have activating functions (see references in main text).

Supplemental References

Blazquez, M. A., and Weigel, D. (1999). Independent regulation of flowering by phytochrome B and gibberellins in Arabidopsis. Plant Physiol *120,* 1025-1032.

Cerdan, P. D., and Chory, J. (2003). Regulation of flowering time by light quality. Nature *423,* 881-885.

Corbesier, L., Gadisseur, I., Silvestre, G., Jacqmard, A., and Bernier, G. (1996). Design in *Arabidopsis thaliana* of a synchronous system of floral induction by one long day. Plant Journal *9*, 947-952.

Corbesier, L., Vincent, C., Jang, S., Fornara, F., Fan, Q., Searle, I., Giakountis, A., Farrona, S., Gissot, L., Turnbull, C., and Coupland, G. (2007). FT protein movement contributes to long-distance signaling in floral induction of Arabidopsis. Science *316*, 1030-1033.

Hayama, R., and Coupland, G. (2004). The molecular basis of diversity in the photoperiodic flowering responses of Arabidopsis and rice. Plant Physiol *135*, 677-684.

Hayama, R., Yokoi, S., Tamaki, S., Yano, M., and Shimamoto, K. (2003). Adaptation of photoperiodic control pathways produces short-day flowering in rice. Nature *422*, 719-722.

Imaizumi, T., Tran, H. G., Swartz, T. E., Briggs, W. R., and Kay, S. A. (2003). FKF1 is essential for photoperiodic-specific light signalling in Arabidopsis. Nature *426*, 302-306.

Jang, S., Marchal, V., Panigrahi, K. C., Wenkel, S., Soppe, W., Deng, X. W., Valverde, F., and Coupland, G. (2008). Arabidopsis COP1 shapes the temporal pattern of CO accumulation conferring a photoperiodic flowering response. EMBO J *27*, 1277-1288.

Kim, S. K., Yun, C. H., Lee, J. H., Jang, Y. H., Park, H. Y., and Kim, J. K. (2008). OsCO3, a CONSTANS-LIKE gene, controls flowering by negatively regulating the expression of FT-like genes under SD conditions in rice. Planta *228*, 355-365.

Ledger, S., Strayer, C., Ashton, F., Kay, S. A., and Putterill, J. (2001). Analysis of the function of two circadian-regulated CONSTANS-LIKE genes. Plant J *26*, 15-22.

Locke, J. C., Millar, A. J., and Turner, M. S. (2005a). Modelling genetic networks with noisy and varied experimental data: the circadian clock in *Arabidopsis thaliana*. J Theor Biol *234*, 383-393.

Locke, J. C., Southern, M. M., Kozma-Bognar, L., Hibberd, V., Brown, P. E., Turner, M. S., and Millar, A. J. (2005b). Extension of a genetic network model by iterative experimentation and mathematical analysis. Mol Sys Biol *1*, 13.

Pouteau, S., Carre, I., Gaudin, V., Ferret, V., Lefebvre, D., and Wilson, M. (2008). Diversification of photoperiodic response patterns in a collection of early-flowering mutants of Arabidopsis. Plant Physiol *148*, 1465-1473.

Somers, D. E., Kim, W. Y., and Geng, R. (2004). The F-box protein ZEITLUPE confers dosage-dependent control on the circadian clock, photomorphogenesis, and flowering time. Plant Cell *16*, 769-782.

Suarez-Lopez, P., Wheatley, K., Robson, F., Onouchi, H., Valverde, F., and Coupland, G. (2001). CONSTANS mediates between the circadian clock and the control of flowering in Arabidopsis. Nature *410*, 1116-1120.

Valverde, F., Mouradov, A., Soppe, W., Ravenscroft, D., Samach, A., and Coupland, G. (2004). Photoreceptor regulation of CONSTANS protein in photoperiodic flowering. Science *303*, 1003-1006.

Wilczek, A. M., Roe, J. L., Knapp, M. C., Cooper, M. D., Lopez-Gallego, C., Martin, L. J., Muir, C. D., Sim, S., Walker, A., Anderson, J., *et al.* (2009). Effects of genetic perturbation on seasonal life history plasticity. Science *323*, 930-934.

Yanovsky, M. J., and Kay, S. A. (2002). Molecular basis of seasonal time measurement in Arabidopsis. Nature *419*, 308-312.

Table S1. Data provenance and file names.

Publications that provided the mRNA waveforms are listed below. The numerical values of the cognate data sets are available as supplemental data in the draft CSBE standard format. Each waveform is assigned a name, including the genotype and experiment number. Corresponding *CO* and *FT* waveforms share the same experiment number. Levels were measured by RT-PCR, with detection either by real-time fluorescence labelling or by hybridisation of radio-labelled probes. The mRNA used as a constitutive control for inter-sample normalization varies. Primers that amplify *UBIQUITIN* (*UBQ*) transcripts (Blazquez and Weigel, 1999) were used in experiments 1-12 and similar primers (Cerdan and Chory, 2003) for experiments 13 and 14. Experiment 15 (Somers et al., 2004) used *ACTIN*2 (*ACT2*). In one experiment, the ratio *FT/CO* was quantified directly (Valverde et al., 2004). Notes: LD – long days; SD – short days; a plus sign indicates wild-type genotype.

Reference	Fig.	Acce-ssion	Geno-type	Period of light-dark cycle	Photo-period (L:D)	RNA tested	Waveform Name	Note
Suárez-López *et al*. (2001) *Nature* **410:**1116-1120	2d	Ler	+	24	16:8	*CO/UBQ10*	co11	LD
	2f	Col	+	24	16:8	*CO/UBQ10*	co12	LD
	3c	Ler	+	24	16:8	*FT/UBQ10*	ft11	LD
	3d	Ler	*35S::CO*	24	16:8	*FT/UBQ10*	ftcoox1	LD
	3e	Col	+	24	16:8	*FT/UBQ10*	ft12	LD
Yanovsky & Kay (2002) *Nature* **419:**308-312	1a	Ler	+	24	8:16	*CO/UBQ10*	co1	SD
		Ler	*toc1-1*	24	8:16	*CO/UBQ10*	co1toc1	SD
	1b	Ler	+	21	7:14	*CO/UBQ10*	co2	
		Ler	*toc1-1*	21	7:14	*CO/UBQ10*	co2toc1	
	1c	Ler	+	24	16:8	*CO/UBQ10*	co3	LD
		Ler	*toc1-1*	24	16:8	*CO/UBQ10*	co3toc1	LD
	1d	Ler	+	21	14:7	*CO/UBQ10*	co4	
		Ler	*toc1-1*	21	14:7	*CO/UBQ10*	co4toc1	
	2a	Ler	+	24	8:16	*FT/UBQ10*	ft1	SD
		Ler	*toc1-1*	24	8:16	*FT/UBQ10*	ft1toc1	SD
	2b	Ler	+	21	7:14	*FT/UBQ10*	ft2	
		Ler	*toc1-1*	21	7:14	*FT/UBQ10*	ft2toc1	
	2c	Ler	+	24	16:8	*FT/UBQ10*	ft3	LD
		Ler	+	24	16:8	*FT/UBQ10*	ft3toc1	LD
	2d	Ler	+	21	14:7	*FT/UBQ10*	ft4	
		Ler	+	21	14:7	*FT/UBQ10*	ft4toc1	
	3	Ler	+	24	8:16	*CO/UBQ10*	co5	SD

	3	Ler	+	30	10:20	*CO/UBQ10*	co6	
	3	Ler	+	24	8:16	*FT/UBQ10*	ft5	SD
	3	Ler	+	30	10:20	*FT/UBQ10*	ft6	
	4c	Ler	+	24	16:8	*FT/UBQ10*	ft7	LD
	4d	Ler	+	24	16:8	*CO/UBQ10*	co7	LD
Cerdan & Chory (2003). *Nature* **423:**881-885	3b	Col	+	20	16:4	*FT/UBQ10*	ft13	
	3b	Col	+	20	16:4	*CO/UBQ10*	co13	
	3d	Col	+	16	9:7	*FT/UBQ10*	ft14	
	3d	Col	+	16	9:7	*CO/UBQ10*	co14	
Imaizumi *et al*. (2003). *Nature* **426:**302-306	2c	Col-0	+	24	16:8	*CO/UBQ*	co8	LD
	2c	Col-0	*fkf1-2*	24	16:8	*CO/UBQ*	co8fkf1	LD
	2d	Col-0	+	24	8:16	*CO/UBQ*	co9	SD
	2e	Col-0	*fkf1-2*	24	8:16	*CO/UBQ*	co9fkf1	SD
	2e	Col-0	+	24	16:8	*FT/UBQ*	ft8	LD
	2e	Col-0	*fkf1-2*	24	16:8	*FT/UBQ*	ft8fkf1	LD
	2f	Col-0	+	24	8:16	*FT/UBQ*	ft9	SD
	2f	Col-0	*fkf1-2*	24	8:16	*FT/UBQ*	ft9fkf1	SD
	S6a	Ler	+	24	16:8	*CO/UBQ*	co10	LD
	S6b	Ler	+	24	16:8	*FT/UBQ*	ft10	LD
Somers *et al*. (2004) *The Plant Cell* **16:**769-782	8a	Col C24	+	24	16:8	*CO/ACT2*	co15	LD
	8b	Col C24	+	24	16:8	*FT/ACT2*	ft15	LD
Valverde *et al*. (2004). *Science* **303:**1003-1006	S2	Ler	*35S::CO*	24	8:16	*FT/CO*	ftcoox2	SD
		Ler	*35S::CO*	24	16:8	*FT/CO*	ftcoox3	LD

Table S2: predictions from the models.

Specific predictions, gaps in data and future experiments highlighted by the models are listed. Many additional predictions (the values of the parameters, for example) and gaps in data (quantitative time series of protein accumulation in the wild type, for example) are generic and are not listed here.

	Prediction or Gap	Model	Outcome	Possible experiments
1	Prediction and Gap	1	Effectiveness of *CO* mRNA in activating *FT* is reduced by ~60% in the first 5h of light in long photoperiods, but less in short photoperiods. This avoids a morning peak of *FT* expression. The effect of *FKF1* (see 6, below) is a possible mechanism.	Identify unknown factor that modifies *FT* activation in this pattern, e.g. quantify CO protein levels in WT compared to mRNA.
2	Prediction	1	*TOC1* has little (40% or less) effect on the light activation of *FT* transcription; *toc1*'s main effect on photoperiodism is *via* the rhythm of *CO* transcription.	Quantify *FT* mRNA levels in response to light in *toc1* and wild type.
3	Prediction	2	The phase of circadian regulation of the *CO* mRNA changes significantly under different photoperiods, similar to *TOC1* in the interlocking-loop model.	Test *CO* mRNA phase under a range of photoperiods, compared to other clock genes.
4	Gap	2	Insufficient data on the phases of clock components under different photoperiods.	As for point 3, above.
5	Prediction	2	The waveform of *CO m*RNA is modified by *FKF1,* which mediates up to a 45% increase in *CO* transcription rate over the last 8h of a long photoperiod, with much less effect in SD. The effect on *CO m*RNA turns on and off sharply. This creates the photoperiod- and *FKF1*-dependent shoulder in *CO* expression.	As for point 3, above, with additional tests in *fkf1.*
6	Prediction and Gap	3, 3F2	*FKF1* very strongly promotes *FT* transcription (~10-fold increase in transcription rate at the end of a long photoperiod).	Test *FKF1* association with *FT* promoter.
7	Prediction	2,3	The *FKF1* effect on *FT* is similar to the effect on *CO* (see 5), for example in its photoperiod-dependence. Both effects of *FKF1* might have similar mechanisms.	Testing *CO* mRNA under LD in *co* mutants showed no effect on the *FKF1*-dependent shoulder

			One hypothesis was that both were mediated by CO protein.	(sup. figure 8).
8	Prediction	3	Discrimination between long and short photoperiods will be optimal for cycle durations close to 24h; short photoperiods are partially inductive in longer or shorter cycles.	Measure flowering time under a range of different photoperiods, each in a range of cycle durations.
9	Gap	4	Insufficient data to quantify the non-linear response of flowering time to *FT.*	Measure *FT* expression profiles and flowering time under a range of photoperiods.
10	Prediction	4	The response measured in 9 will be approximated by equations (10, 11), up to the latest flowering times shown (sup. Figure 6). Later flowering times cannot yet be predicted.	As for point 9, above.